Microchemical Analysis in the SEM

7

In most cases, it is desirable to obtain chemical information from specimens that are examined in the SEM. This is usually accomplished using energy dispersive x-ray spectrometry (EDS) or wavelength dispersive x-ray spectroscopy (WDS) technique. The microchemical analysis is accomplished by EDS detector or WDS spectrometer fitted in the column of the SEM. Integration of this detector or spectrometer with the SEM enables a user to determine the localized chemistry of a region. For example, the microchemical make-up of features that are only a few microns in size can be determined with a high degree of sensitivity. Not only the elements that make up a phase are detected (qualitative analysis) but also their concentrations are determined (quantitative analysis). The microchemical analysis is efficient and nondestructive and thus plays an important role in materials verification and phase identification. The EDS detector and WDS spectrometer are incorporated into the SEM in a way that does not disturb or affect the imaging capability of the instrument. The EDS and WDS identify the quantum characteristic x-ray energy and wavelength, respectively for elemental analysis. Their mode of operation is controlled by computers. This chapter describes the techniques used to undertake microchemical analysis in the SEM.

7.1 Energy Dispersive X-Ray Spectroscopy (EDS)

Interaction of primary electron beam with the specimen material results in the generation of characteristic x-rays and white radiation (background x-rays) which collectively form an x-ray signal. An x-ray detector is used to collect x-ray signal, measure its energy and intensity distribution, and analyze it in a manner that identifies elements and determines their respective concentrations in the analyzed region of the specimen material. Most commonly used x-ray detector in the SEM is the energy dispersive x-ray spectrometer (EDS).

A. Ul-Hamid, *A Beginners' Guide to Scanning Electron Microscopy*,
https://doi.org/10.1007/978-3-319-98482-7_7

Historically, Fitzgerald [1] successfully demonstrated the use of an EDS detector coupled to an electron microprobe analyzer. The resolution of EDS detectors at the time was no better than 500 eV which has now improved to 122 eV (using Mn k_α as reference peak) making most of the present-day microchemical analysis possible. In the past, energy dispersive x-ray spectrometers coupled with the SEM were primarily single-crystal Si(Li) (lithium-drifted Si) solid-state semiconductor devices. At present, however, Si drift detectors (SDD) have become commonplace. A photograph of a modern-day EDS detector used with the SEM is shown in Fig. 7.1a. The output of an EDS detector in the form of an EDS spectrum is shown as an example in Fig. 7.1b.

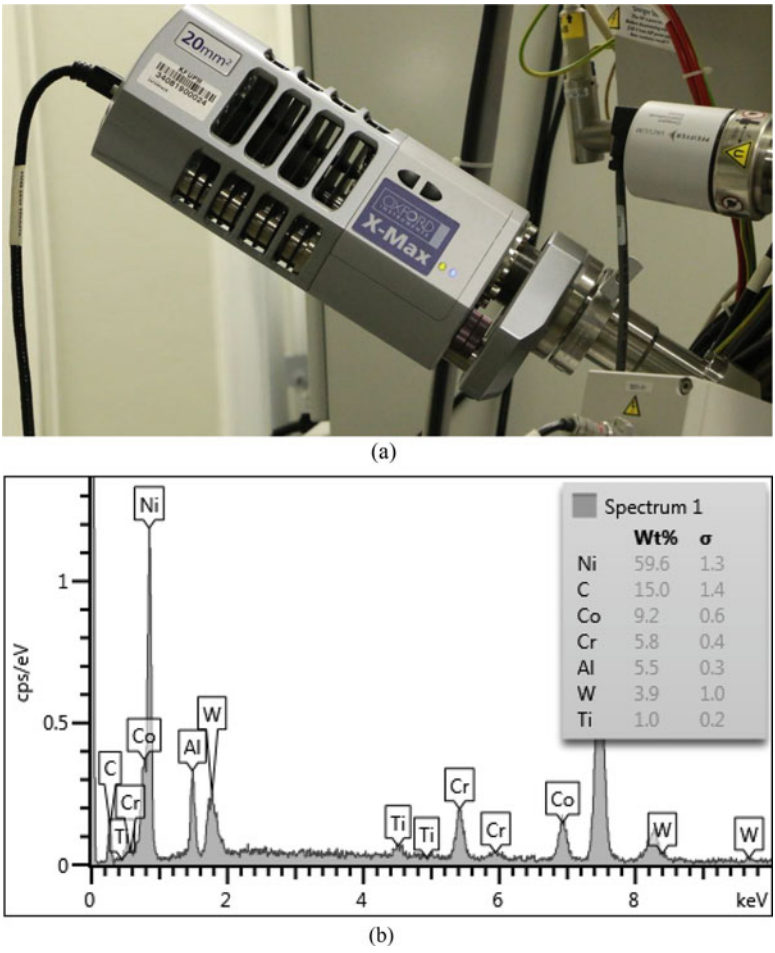

Fig. 7.1 (**a**) Photograph of Peltier-cooled EDS detector mounted on an SEM. (**b**) Energy dispersive x-ray spectrum obtained from a high-temperature Ni-based alloy showing the presence of various elements

7.1.1 Working Principle

A schematic diagram of the EDS detector setup commonly used in the SEM is shown in Fig. 7.2a. X-rays cannot be deflected into the detector thereby restricting collection to only those x-rays that are in line-of-sight of the detector. For this reason, the detector needs to be placed as close to the specimen as possible to increase the efficiency of x-ray collection. The distance between the specimen and the detector is normally 20 mm. X-rays emanating from a specimen are collected by a collimator tube which is located at the front end of the detector. The collimator acts as a limiting aperture and ensures that x-rays that originate only from the specimen are collected while stray x-rays from the specimen chamber or backscattered electrons do not find their way into the detector. Collimators can come in various shapes. One typical design is shown in Fig. 7.2b. A pair of permanent magnets is placed after the collimator to deflect any incoming electrons that can cause background artifacts in the x-ray spectrum.

Following the electron trap, there is a thin opaque window which serves to isolate the environment of the SEM chamber from the detector (see Fig. 7.2a). The window is followed by a semiconductor crystal that is sensitive to light. Thin window acts as a shield to protect the crystal from visible radiation. It also forms a barrier to maintain a vacuum within the detector assembly. Until 1982, the only available window was made of beryllium. Due to its high mechanical strength, Be window did not require a support structure. However, lack of support necessitated the use of a thick (around 8 μm) window which would absorb x-rays of energy less than 1 keV, thus preventing the detection of light elements such as boron, oxygen, nitrogen, carbon, etc. To enable light elements detection, an "ultrathin" window (UTW) made of thin (tens to a few hundred nanometers) organic film Formvar coated with gold was used instead of beryllium. This window is unable to withstand atmospheric pressure, and the detector assembly is kept under vacuum. The window can be removed altogether, and the detector can be used in a "windowless" mode. However, this leaves the detector exposed to contamination. In this situation, if the SEM chamber is vented, hydrocarbon condensation and ice formation will occur on the detector surface. The light will also be transmitted onto the semiconductor surface.

Presently, the ultrathin window of polymer covered with a thin layer of evaporated Al and supported with Si grid at the detector side is used as a standard. Due to grid support, the window is able to withstand the pressure of >100 Pascal in the SEM chamber. Support structure blocks part of the low-energy radiation thus reducing the detector efficiency to some extent. The grids are therefore designed to have up to 80% area available for x-ray transmission. This type of window can transmit low-energy (≈100 eV) x-rays and is a preferred choice for light element analysis. Evaporated Al coating serves to restrict the passage of light through the polymeric material which otherwise exhibits high optical transparency. More recently, SiN [2, 3] and graphene [4, 5] have been investigated as potential window materials. Modern EDS detectors routinely detect elements from beryllium to uranium. First three elements of the periodic table H, He, and Li are not detected since they do not have enough electrons to produce characteristic x-rays.

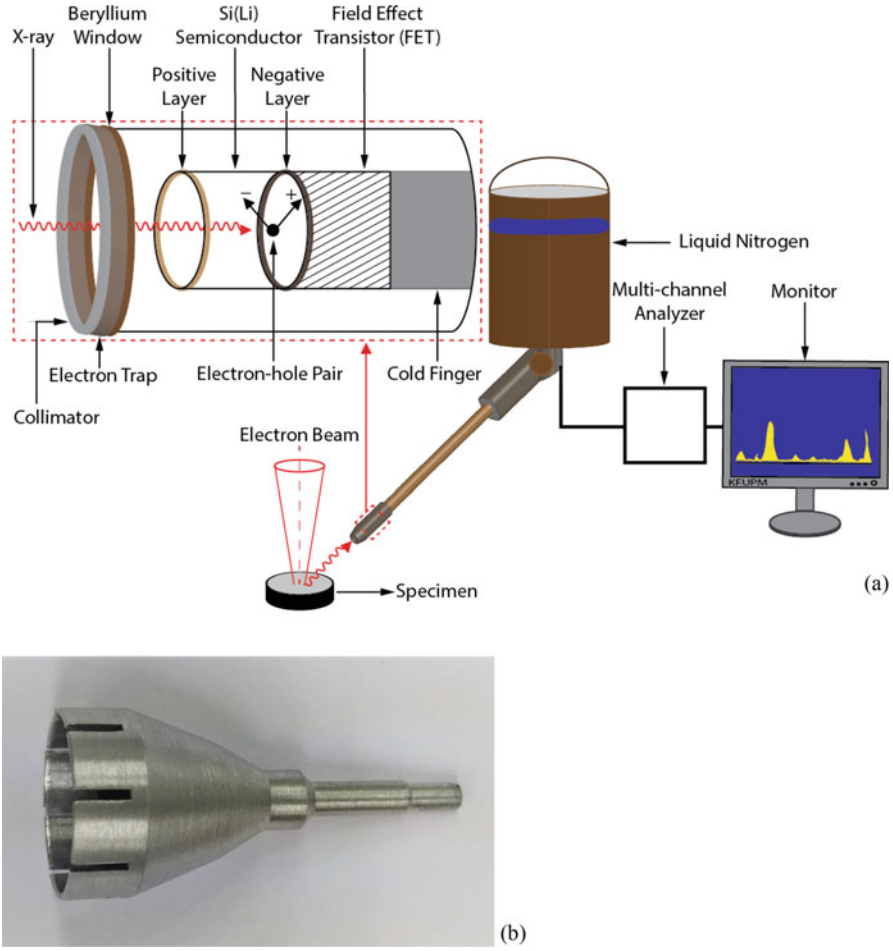

Fig. 7.2 (**a**) A schematic diagram of the EDS detector setup commonly used in the SEM. X-rays emanating from the specimen enter the EDS detector assembly through a tube called the collimator. (**b**) Photograph of a typical collimator assembly used to collect x-rays in the EDS detector

X-rays emanating from the specimen pass through thin window shield and reach the semiconductor diode detector made of single crystal of Si (or Ge). The energy gap between valence and conduction band is relatively small in semiconductors (1.1 eV in Si). X-ray photons striking the detector surface ionize Si atom through photoelectric effect creating electron-hole pairs (Fig. 7.3a). Upon application of a bias voltage between the thin gold contacts present at opposite ends of the semiconductor, these electrons and holes move in opposite directions toward the collection electrodes. The negative bias voltage applied to the front contact drives the electrons to the back contact and into the field-effect transistor (FET). This flow of current between the electrodes takes about 1 μs and is referred to as a charge pulse

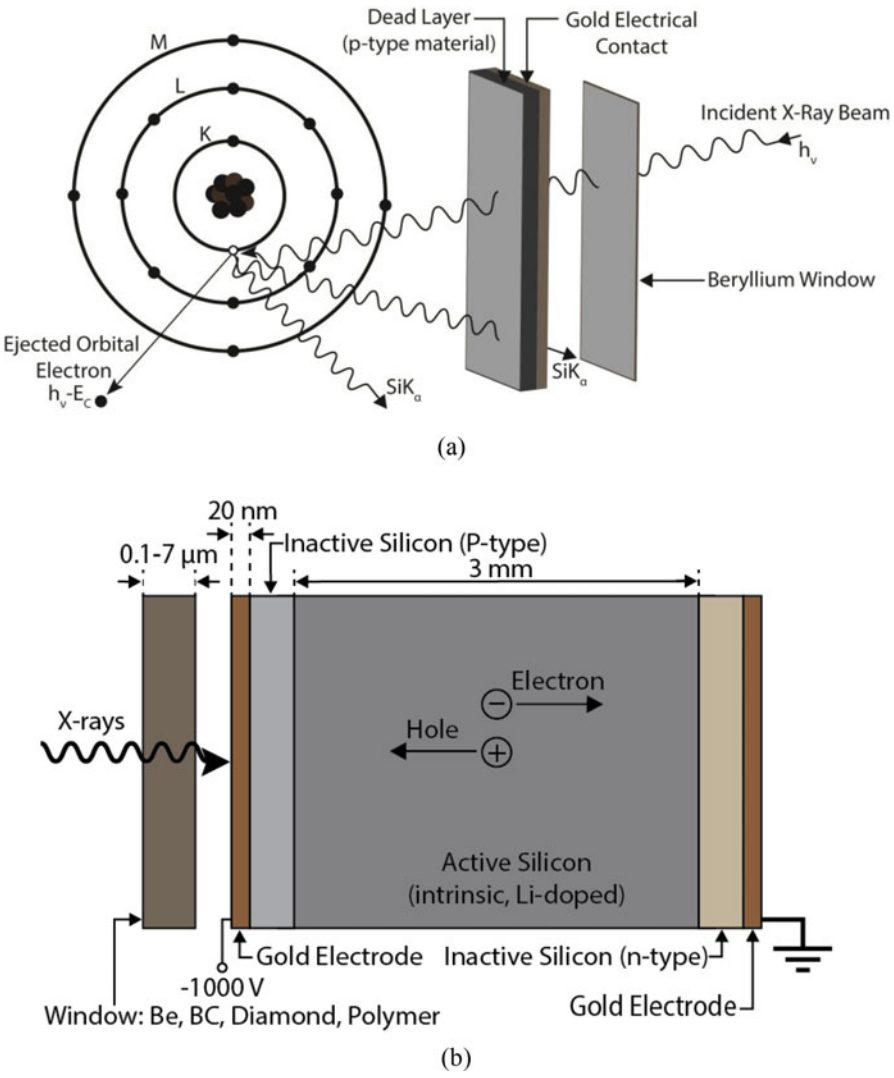

Fig. 7.3 (**a**) X-rays pass through thin window that protects the detector surface from visible radiation. Interaction of the x-rays with the Si(Li) detector results in the generation of electron-hole pairs whose number is proportional to the energy of the x-ray photons. (**b**) Schematic illustrating the working of p-i-n junction reversed biased semiconductor detector. Electrons and holes move in opposite directions and result in the generation of a pulse. The number of pulses is counted and correlated to the energy of the photons which created these pulses. Elements are identified since these generate photons with unique energy values

(Fig. 7.3b). The higher the energy of the x-ray photons that arrive from the specimen, the greater is the number of the charge pulses generated. Thus, the electrical charge that flows through the semiconductor is proportional to the number of electron-hole

pairs created. The mean energy required to create one electron-hole pair (one electric pulse) in undoped Si is taken as 3.86 eV. The number of charge pulses generated in the detector can be counted, and the x-ray photon energy responsible for this pulse output is calculated by multiplying this number by 3.86. For instance, if the pulse output count is 1642, the x-ray energy that would produce such a number will be $1{,}659 \times 3.86 = 6{,}403$ eV or 6.4 keV. This energy corresponds to K_α x-ray line which is emitted when an electron transitions from L to K shell in the Fe atom. The energy value is fixed for this particular transition and thus whenever a magnitude of pulse equaling the number of 1,659 is measured; Fe is identified as a possible constituent of the specimen under examination. The greater the number of times this particular value of pulse count is generated, the higher is the elemental concentration of Fe in the material. Similarly, Ni K_α and Al K_α x-rays will generate 1,927 and 385 electron-hole pairs, respectively, as a result of ionization within the Si semiconductor. Since each element has unique characteristic x-ray energies that are different than other elements, they can be identified by measuring the magnitude of the pulse height.

Lithium is added in Si to make lithium-drifted silicon or Si(Li) detectors since, in practice, it is not possible to make a good intrinsic semiconductor from pure Si. Lithium, if added in the correct amount, serves to reduce defects present in the Si lattice. The aim is to create a large charge-free zone in the semiconductor using Li which compensates for charge carriers created by impurities. In this manner, the only charge exhibited by the semiconductor is generated by the incoming x-ray photons. Lithium is an *n*-type dopant and forms a *p-n* junction upon application onto pure Si. Addition of Li ensures that the maximum number of x-ray photons is used to generate charge pulses in the detector. One disadvantage is that upon application of high voltage bias, the Li is pulled toward the biased electrode giving rise to electronic noise. Cooling of the semiconductor by liquid nitrogen limits the mobility of Li ions. Si surface used in a Si(Li) EDS detector is around 3 mm in thickness and provides a maximum working area of 30 mm^2. Any further increase in the size of the detector increases noise.

The charge pulse created at this stage is small with large noise making it impossible to measure the energy of the x-ray photon. The Si(Li) crystal is connected to a FET at the rear end (Fig. 7.2a), which acts as the preamplifier to increase the signal strength and signal-to-noise ratio. The charge pulse created by the electron-hole pairs is converted into voltage steps (in mV) with the help of the preamplifier. The output of the FET is in the form of a *staircase waveform*. The size of a voltage step is proportional to the energy of the x-rays incident on the detector surface and the number of electron-hole pairs created. The voltage step is converted into a signal pulse by a pulse processor. The height of the signal pulse is proportional to the voltage step or to the energy of the photon striking the diode surface. The signal is averaged to reduce noise and improve pulse shape. An analog-to-digital converter (ADC) is used to convert pulses with various heights into pulses with constant heights. A number of pulses created is proportional to the heights of the input pulses. This process is known as *pulse height analysis* (PHA). The peak height of each signal pulse is converted into a digital value and assigned to the appropriate channel

in a computer *multichannel x-ray analyzer* (MCA) which displays the data in the form of a plot between voltage and intensity. The voltage range (displayed as units of energy, e.g., 10 keV, 20 keV, etc.) on the *x-axis* is divided into a number of channels (e.g., 1024, 2048, etc.). Each channel corresponds to a specific range of energy (e.g., Fe K_α x-ray line is from 6400–6410 eV). In this manner, one count is recorded at that particular energy level. Due to statistical variation in the energy of the electron-hole pairs created, a single peak with a Gaussian profile occupies several channels and can be roughly 150 eV wide. The number of times a particular voltage pulse is generated is plotted as intensity on the *y-axis* in the units of counts or counts per second (Fig. 7.1b).

In addition to the qualitative identification of an element, a quantitative measure of the concentration of that element can be undertaken. This is accomplished by counting the number of times a voltage pulse corresponding to a particular characteristic x-ray photon is generated and received in a channel of MCA reserved for that energy. The higher the count, the higher is the elemental concentration within the specimen volume analyzed. The higher the intensity of a peak, the greater is the concentration of element represented by that peak. The process of pulse generation, counting, identification of an element, and measurement of concentration is more or less automated in most cases. Output can be printed in the form of a labeled x-ray spectrum or transferred as data files onto another storage device such as a USB memory device.

The semiconductor crystal needs to be kept cool (at around −140 °C) to function properly; otherwise, electron-hole pairs are created at room temperature without any bombardment of x-ray photons. This will result in the addition of electronic noise to the x-ray spectrum. Cooling is usually achieved by mounting the detector and FET onto a cold finger (copper rod) that is connected to a Dewar of liquid nitrogen (LN_2) kept at −195.80 °C (Fig. 7.2a). Liquid nitrogen needs to be replenished every few days. Liquid nitrogen-free detectors such as Peltier-cooled (Fig. 7.1a) have become popular. The whole assembly is kept under vacuum at all times to avoid picking up contamination from the SEM chamber. The vacuum helps to maintain a low temperature as well. Water vapor and hydrocarbon molecules present within the SEM chamber are prevented from condensing on the surface of the semiconductor device by the thin window mounted before the diode. To avoid damage, a detector is not to be used in a "warmed-up" condition or if the vacuum is not present. A temperature sensor switches off the bias voltage if the detector is warm. The detector is constructed in a way that the semiconductor crystal and the cold finger are separated from the housing assembly. Retractable EDS detectors are usually employed whereby it is possible to move the detector close to and away from the specimen without breaking the vacuum in the SEM chamber.

Improvement in silicon detector technology has allowed the development of silicon drift detectors (SDD) where *n*-type large-area silicon wafer receives the incoming x-rays. The other side of the Si is decorated with concentric shallow rings of *p*-type drift material surrounding a small central anode contact. Upon application of bias, electrons *drift* through a field gradient that exists between the concentric rings and are collected at the central anode. These detectors are cooled

using moderate thermoelectric cooling (e.g., Peltier technology) thus eliminating the need to use liquid nitrogen as a coolant. These detectors exhibit faster analysis times with higher count rates compared to conventional detectors. High count rates are possible due to the large surface area (up to 100 mm^2) of semiconductors used in SDD enabling fast data collection. Surface area in conventional Si(Li) detectors is limited to 30 mm^2 due to an increase in anode capacitance and noise with an increase in size. Larger sensors are possible with SDD detectors giving a superior resolution. The main disadvantage of these detectors is low detectability of light elements due to the presence of noise at low energies of the x-ray spectrum. The large size of the detector necessitates an equally large port opening in the SEM chamber which reduces flexibility in equipment design.

7.1.2 Advantages/Drawbacks of EDS Detector

It is common to find an EDS detector attached to an SEM due to its large number of advantages. An EDS detector is simple, robust, versatile, easy-to-ease and do not take up a large amount of space. Its functionality is seamlessly integrated into SEM operation. It undertakes a simultaneous analysis of all elements. The high efficiency of the detector combined with the large solid angle of collection (typically 0.5 steradian) results in small analysis time (e.g., less than 1 min). Due to this reason, low probe currents can be employed to extract elemental information from sensitive specimens. EDS technique is sensitive to light elements (can detect Be and higher) and can efficiently perform quantification of elemental data. The working distance setting when using EDS is not as critical as it is for WDS.

Disadvantages include low-energy resolution (122 eV) compared to wavelength dispersive x-ray spectrometer due to which closely spaced x-ray peaks cannot be distinguished, low detectability of elements (0.1–0.2 wt%) compared to WDS (0.001–0.002 wt%), low sensitivity to minor/trace elemental concentrations and lighter elements, and decreased resolution at high count rates.

7.2 Qualitative EDS Analysis

Qualitative EDS analysis is the identification of elements present within a specimen using energy dispersive x-ray spectroscopy. Qualitative EDS analysis in the SEM is a powerful tool that quickly determines the microchemical constituents of a specimen in a nondestructive manner. Since the x-ray signal resulting in an EDS spectrum is generated from a limited (in the order of microns) volume of material, it can be used to identify heterogeneity or segregation in specimens and also determine the chemistry of small objects or areas of interest.

7.2.1 Selection of Beam Voltage and Current

The SEM-EDS analysis is conducted by selecting a region of interest in the specimen. Usually, a high accelerating voltage (such as 20 kV) is selected for EDS analysis in order to provide adequate energy to the primary beam for it to excite characteristic x-rays of all elements of interest within 0–15 keV spectrum range. Occasionally, it is necessary to acquire spectrum up to 20 keV range for which higher beam energies (e.g., 30 keV) are required. Higher beam energies allow for higher peak intensities and a complete coverage of x-ray peaks from light to heavy elements. However, at the same time, it increases specimen interaction volume hence decreasing x-ray spatial resolution and increasing absorption. Generally, a primary energy of 2.7 times greater than critical excitation energy of a particular x-ray peak is optimum for analysis. Similarly, the probe current used during EDS analysis is usually higher than that recommended for imaging. These two parameters need to be considered in conjunction with the specimen's ability to resist beam damage since higher voltages and currents and longer analysis time increase the probability of contamination and beam-induced specimen damage.

7.2.2 Peak Acquisition

The whole EDS spectrum usually up to 20 keV can be acquired within approx. 100 s. The computer checks peak energies against values of characteristic x-ray energies for different elements saved in its database and can label these peaks with the names of the elements during the acquisition process itself. Most of the major (high-intensity) peaks are automatically identified quickly in this manner. Minor (low intensity) peaks may need some operator input. Thus, from a user's point of view, the process of acquisition and qualitative analysis of x-ray spectra is efficient and fairly straightforward. However, it is necessary to understand the process behind this identification in order to be able to verify results and also resolve any complications arising due to any overlapping or low-intensity peaks and artifacts in the spectrum.

7.2.3 Peak Identification

In an EDS spectrum, *x*-axis displays x-ray energy in keV, and the *y*-axis shows intensity in counts or counts per second as shown in a typical EDS spectrum shown in Fig. 7.4. Different peaks are positioned at different x-ray energies. Elements are identified on the basis of their peak positions or x-ray energies. For instance, a peak occurring at 7.47 keV is identified as Ni K_{α} as it is known that the latter falls at this specific position. In order for peak positions to be accurately identified, it is necessary that EDS is properly calibrated which is done by using a pure metal standard such as Ni. Once the EDS spectrum is acquired by the computer, the

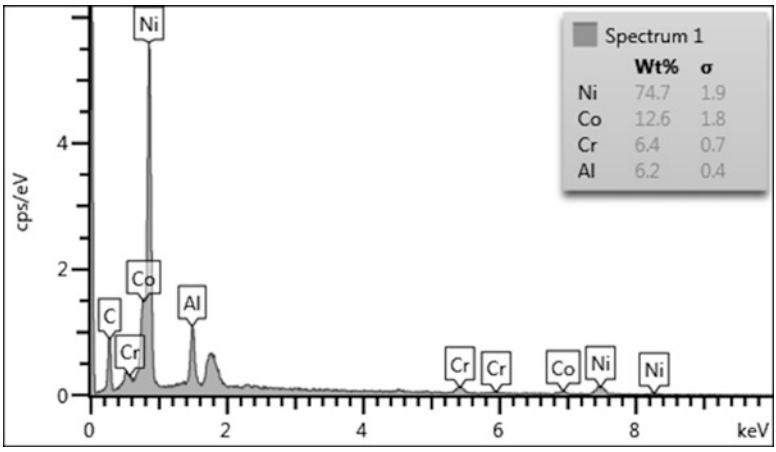

Fig. 7.4 Typical EDS spectrum a showing plot of intensity (counts or counts per second, cps) on *y*-axis and energy of emitted x-ray photons (keV) on the *x*-axis. Quantified elemental concentration is shown in the inset

specific energy of each characteristic x-ray peak is determined and compared with the values present in the database. The database has reference peak values stored for all elements. Most of the times, this database suffices for peak identification. Peaks are identified automatically by the computer, or it can be overridden by the user. With increasing atomic number, the number of peaks emanating from elements also increases. Heavy elements give rise to a large number of x-ray peaks. In order to identify a given element with confidence, most of this family of peaks need to be identified. Detection of a single peak for a particular element may lead to erroneous identification. All peaks belonging to a particular element need to be sought. Acquired spectra are stored in the computer and can be processed at any time later to reconfirm analysis or reassign peak identities, if necessary.

Peak intensity should be at least three times the intensity of the background in order to be identified properly. If necessary, analysis time is increased to acquire adequate peak height. Peaks falling at the high-energy end of the spectrum are identified first as they are more widely separated and easily determined. High-intensity peaks are identified as K_α, L_α or M_α depending on atomic numbers of elements present in the specimen. This is followed by the identification of corresponding K_β, L_β, or M_β whose intensity is many times lower. Next, low-energy peaks are identified. EDS detector's resolution at low-energy end is less, therefore restricting the number of peaks originating from light elements to one only. This end of the spectrum will also have L peaks for elements displaying corresponding K peaks at higher-energy end. If the low concentration of elements are present and need to be identified, then a spectrum with very high counts need to be acquired by increasing the analysis time.

7.2.4 Peak to Background Ratios

The high peak-to-background ratio in the EDS spectrum is desirable as it increases the detectability limit of elements. Small probe size generally results in high peak-to-background ratio, which also increases with increasing values of $E_0 - E_c$ where E_0 is the primary beam energy and E_c is the critical excitation energy of x-ray line. However, E_0 can only be increased to an optimum level beyond which the beam will travel to a greater depth within the specimen deteriorating the spatial resolution and increasing x-ray absorption. This will in turn decrease the number of x-ray photons emitted from the specimen and degrade the detectability limit. Therefore, an overvoltage of 2–3 times is optimum for most materials.

7.2.5 Background Correction

Both characteristic and continuum intensities make up the x-ray spectrum. Gaussian peak tail extends over a substantial range of energy and interferes with the adjacent background. Therefore, measurement of background becomes difficult due to the challenge of pinpointing its exact level adjacent to the peak under observation. This situation becomes more complex for a mixture of elements which also cause less accurate interpolation. Background correction is undertaken by the software as follows:

Background Modeling Continuum energy distribution function can be measured and also calculated. It is then combined with a mathematical description of the detector response function which is used to find the background. Finally, subtraction from detected spectral distribution is undertaken.

Background Filtering Mathematical filtering or modification of frequency distribution is also used for background removal. Digital filtering and Fourier analysis are examples of this method.

7.2.6 Duration of EDS Analysis

Length of analysis can be 10–100 s depending on the required strength of the x-ray signal. For major elements, shorter counting times can be used while longer counting times are required for minor or trace element detection. Major elements can display peaks of reasonable intensity in shorter times, while minor elements need longer analysis time to achieve equivalent or reasonable peak intensities. Solid-state detectors are placed close to the specimen thus increasing solid angle for x-ray collection raising count rate and sensitivity to detect the small concentration of elements or light elements in a given acquisition time.

7.2.7 Dead Time

X-rays emanating from the specimen enter into the EDS detector, processed and displayed on the computer in the form of a spectrum. EDS detector's capacity to receive and process x-ray photons is not unlimited. While one x-ray event is received and processed, other simultaneous incoming x-rays are not processed. The duration for which these x-ray signals are not processed is known as *dead time*. The stronger the x-ray signal the longer is the dead time of the detector, i.e., the longer it takes to process x-rays. Dead time appears as a percentage and is normally kept below 25% for efficient analysis. The analysis is usually done in *live time* mode which indicates the duration during which x-ray signals are actually processed. Modern SDD detectors tend to have shorter dead time intervals meaning they can process x-ray signals relatively quickly. The dead time is calculated as follows [6]:

$$\%\text{Dead time} = \left(1 - \frac{\text{Count rate of the output}}{\text{Count rate of the input}}\right) \times 100\% \tag{7.1}$$

Alternatively, it is defined as:

$$\%\text{Dead time} = \left(\frac{\text{Total clock time} - \text{Live time}}{\text{Live time}}\right) \times 100\% \tag{7.2}$$

Live time is the time required for signals collection, and the total clock time is the time required for the signals collection in addition to the signals processing time. The count rate of the spectrum will change depending on the rate of continuous x-rays arriving from the specimen, which varies with the sample's elemental composition resulting in changes in the dead time [7].

7.2.8 Resolution of EDS Detector

The energy resolution of an EDS detector is its ability to distinguish two adjacent peaks in the EDS spectrum. It is measured at full width at half maximum (FWHM) and quoted for a peak at 5.9 keV (Mn K_α) energy position. The energy resolution of present-day EDS detectors is quoted to be around 122 eV. The lower number (in eV units) indicates a higher resolution. Narrow peaks represent better resolution as the overlap between peaks decreases at increasing resolution. Peaks formed by low-energy x-rays show better resolution. For example, in silicon drift detectors, the resolution of the F K_α peak and C K_α peaks is between 60–75 eV and 56–72 eV, respectively. Energy resolution is also related to the live time used when collecting the EDS spectrum. Narrower peak and better resolution are obtained when the process time is long. However, this leads to longer dead time; thus increasing the total time required to acquire the spectrum. Good spectral resolution is desirable in order to identify and quantify the elements present in a specimen.

Electronics used in pulse processing plays an important role in achieving good energy resolution by way of eliminating peak shifts and peak distortions [6]. The

relationship between the EDS detector's energy resolution, the quality of the electronics used, the width of the intrinsic line, and FWHM is expressed as follows [6]:

$$R^2 = I^2 + P^2 + X^2 \tag{7.3}$$

where

R = the detector's energy resolution
I = width of the intrinsic line of the detector
P = indicator of the quality of the electronics used (FWHM of the electronics generating the pulse)
X = the equivalent FWHM related to incomplete charge collection (ICC) and leakage current of the detector

Modern EDS software can automatically measure the resolution. On the other hand, Mn or Cr peaks can be collected with the selection of a proper window that can contain the peaks on both sides. The peaks should include 50% of the maximum count in the channel at the center. Figure 7.5 shows the energy resolution measurement by specifying the number of channels which contain the FWHM of Mn K_α peak for a specific EDS detector.

X-ray lines acquire the shape of a peak since there is a statistical distribution of energies associated with x-ray photons emanating from a given element due to a particular type of transition. Natural width of an x-ray peak is small, but it gets broadened after passing through the EDS detector electronics. Peak broadening leads to a decrease in peak height and peak-to-background ratio which adversely affects

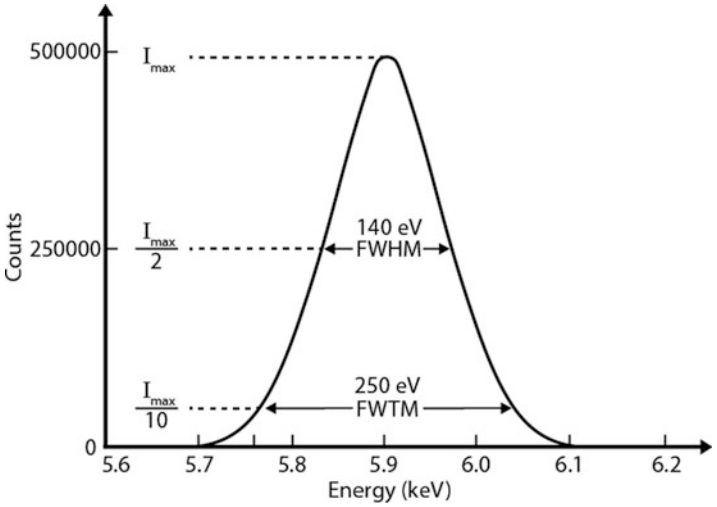

Fig. 7.5 Energy resolution is measured by identifying the channels that encompass the FWHM of Mn K_α peak. Full width at tenth maximum (FWTM) can also be measured which indicates the extent of distortions in the peak [6]

detection of elements in a specimen. It also contributes to peak overlaps since the wider the peaks the greater is the chance that some peaks overlap each other.

7.2.9 Overlapping Peaks

Characteristic x-ray peaks from different elements can have the same energy in which case they will overlap in the EDS spectrum. It is difficult to distinguish between peaks that fall within 100 eV of each other, especially if there is a substantial difference in their heights. Small peaks in the neighborhood of large peaks also present a similar challenge. Frequently encountered overlapping peak pairs include $SK_{\alpha,\beta}$-MoL_{α}, $SK_{\alpha,\beta}$-PbM_{α}, TiK_{α}-BaL_{α}, CrK_{β}-FeK_{α}, MnK_{α}-CrK_{β}, FeK_{α}-MnK_{β}, $WM_{\alpha,\beta}$-$SiK_{\alpha,\beta}$, $TaM_{\alpha,\beta}$-$SiK_{\alpha,\beta}$, YL_{α}-PK_{α}, etc. The user should be aware of these overlaps in order to avoid incorrect peak assignments. Peak overlaps appear as unusually broad peaks or shoulders in large peaks. Peak stripping feature is provided in EDS software which can help strip one peak based on stored peak positions to reveal hidden peaks underneath.

7.3 Artifacts in EDS Analysis

7.3.1 Peak Distortion

Thin "dead" layer present on the Si crystal can lead to self-annihilation of electron pairs resulting in the loss of charge. This can cause peak distortion due to incomplete charge collection (ICC) [7]. The peak will deviate from the Gaussian shape as seen in Fig. 7.6. Heating the detector will reduce the effect of the dead layer on the peak shape.

Peak distortion can also occur due to *background shelf* which is defined as background increments at energy range lower than the peak of concern. The background shelf occurs when continuous x-rays are scattered inelastically and spread out through the detector thus escaping detection. This effect is prominent in the spectra of radioactive materials [7] such as (^{55}Fe) [8] as seen in Fig. 7.7.

7.3.2 Peak Broadening

The number of electron-hole pairs produced for specific energy is not absolute but depends on statistical distribution. The final count shows the average only. This introduces uncertainty leading to the broadening of peaks [8]. Another uncertainty arises from the thermal noise originating from the process of amplification [7]. For photon energy, the Gaussian distribution is used to describe the distribution of the number of charge carriers and is shown in Fig. 7.8. The description is given by the following equation:

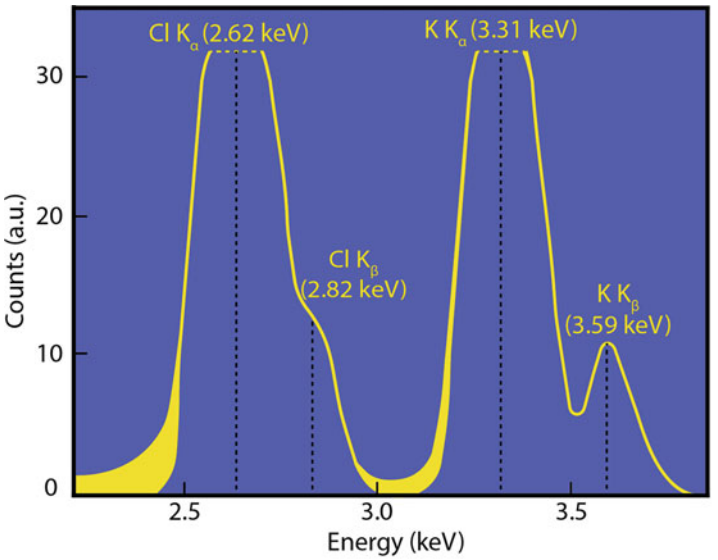

Fig. 7.6 EDS spectrum of potassium chloride with ICC artifacts. The yellow region in the spectrum shows the effect of the incomplete charge collection resulting in the peak deviation from the perfect Gaussian shape [8]

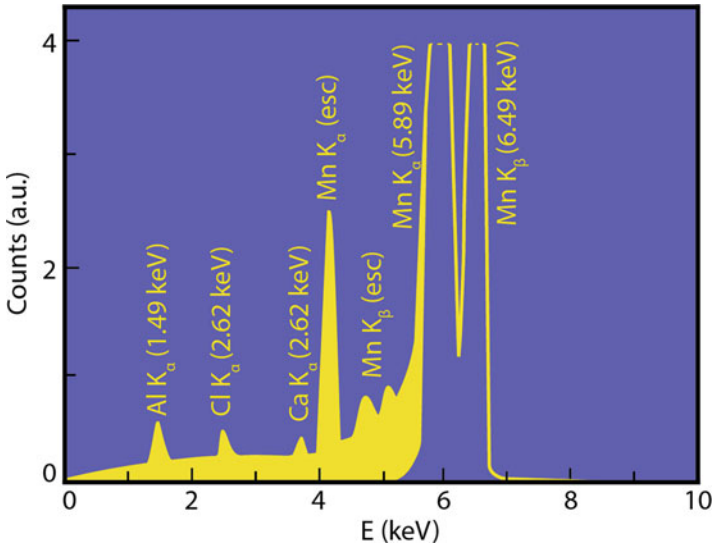

Fig. 7.7 EDS spectrum of radioactive ferrous (^{55}Fe) with background shelf effect visible for the energy range lower than Mn K_α peak [8]

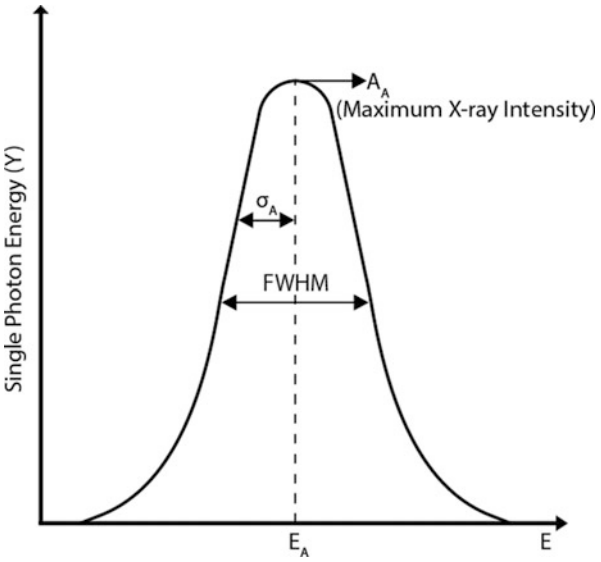

Fig. 7.8 Peaks are defined by Gaussian distribution [8]

$$Y = A_{\mathrm{A}} \exp\left[-\frac{1}{2}\left(\frac{E_{\mathrm{A}} - E}{\sigma_{\mathrm{A}}}\right)^2\right] \tag{7.4}$$

where

Y is the peak intensity
A_{A} is the maximum intensity
E_{A} is the average energy for the peak
E is the energy of the x-ray
σ_{A} is the standard deviation

The standard deviation is used to indicate the broadening of the peak. The relation between the standard deviation and FWHM is given by FWHM $= 2.355\sigma_{\mathrm{A}}$.

Peak broadening decreases peak height (counts) and the peak-to-background ratio [8]. Figure 7.9 shows the effect of peak broadening on Mn K_α peak.

Peaks with similar counts but at different energies may show different heights due to peak broadening effect. This will introduce an error in the estimation of the relative concentration of elements if peak heights are compared [8]. This effect is shown in Fig. 7.10.

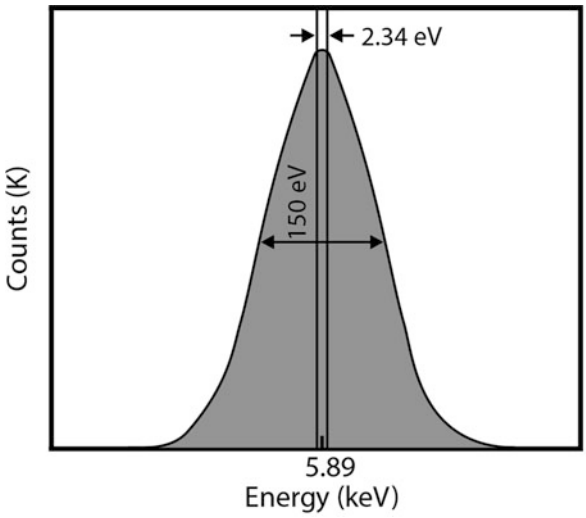

Fig. 7.9 Schematic illustrating the peak broadening effect on the Mn K_α peak. Width increases from 2.34 to 150 eV. Counts are reduced from 1000 to 15 [8]

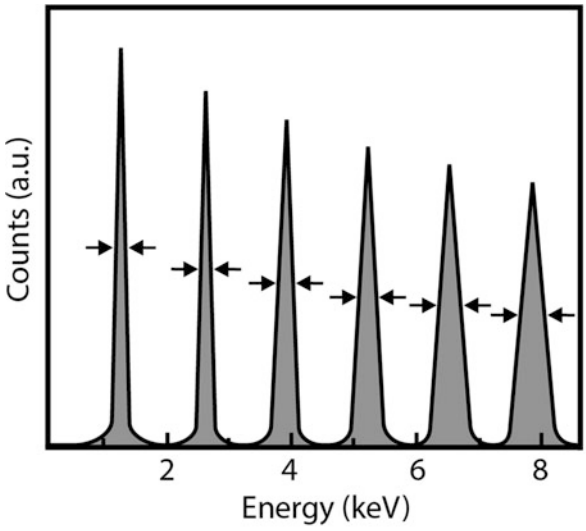

Fig. 7.10 Variation of height in the peaks with different energy but same counts [8]

7.3.3 Escape Peaks

It is statistically possible that x-ray photons emanating from specimen enter the detector and ionize Si releasing K-type x-ray photons. If this transition occurs close to the detector surface, the photons can escape the detector. This will decrease the energy of the x-rays emanating from the specimen by an amount equal to that required for the Si K transition event. Due to this event, an escape peak is generated in the x-ray spectrum at energy $E_{(\text{specimen})}$-$E_{\text{SiK}\alpha}$. For instance, if Cu is the specimen material tested, an escape peak at 8.04 ($E_{\text{CuK}\alpha}$) − 1.74 ($E_{\text{SiK}\alpha}$) = 6.3 keV can form in

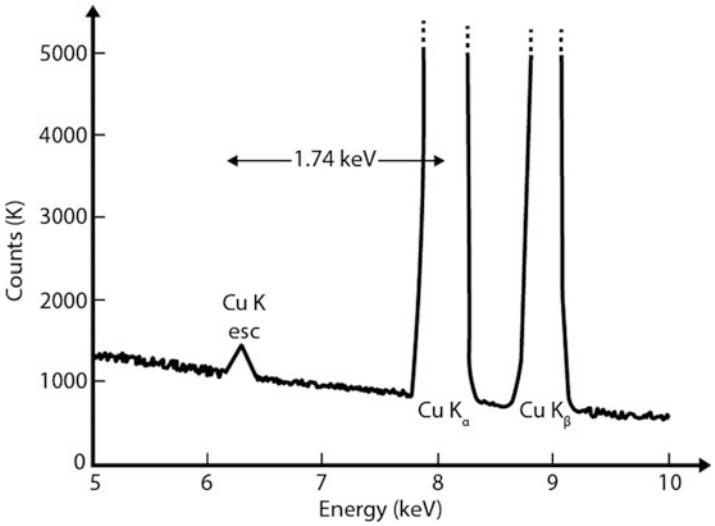

Fig. 7.11 The Cu K_α escape peak forms at an energy of 1.74 keV less than that of Cu K_α

the x-ray spectrum (see Fig. 7.11). The probability of the formation of Si K_β peak is much less than that of Si K_α peak [8].

The fluorescence of the Si can only occur when the incident x-ray energy is greater than that required for the critical excitation of Si. The escape peaks size is typically related to the parent peak (between 1% and 2% of the parent peak) [9]. Since the x-rays emitted from high atomic number atoms will lose energy in greater depths within the detector, hence, in case of Si fluorescence x-rays are produced, they will face difficulties in leaving the detector, thus reducing the escape peaks artifact [10]. The user needs to be aware of this escape peak phenomenon in order to be able to recognize it when it occurs and not to confuse it with some other genuine peak emanating from the specimen.

7.3.4 Sum Peaks

When two characteristic x-rays arrive at the detector simultaneously, the detector might consider them as one and display it at an energy equal to the sum of the energies of the two x-rays. Accumulation of such events might lead to a peak in the spectrum at sum energy position [6, 8, 9, 11]. This peak is known as *sum peak* (or double or coincidence peak) which is an artifact. The sum peaks are more probable to occur when the count rate for the input photons is large and the dead time exceeds 50–60%. Presence of major speaks in the EDS spectrum also

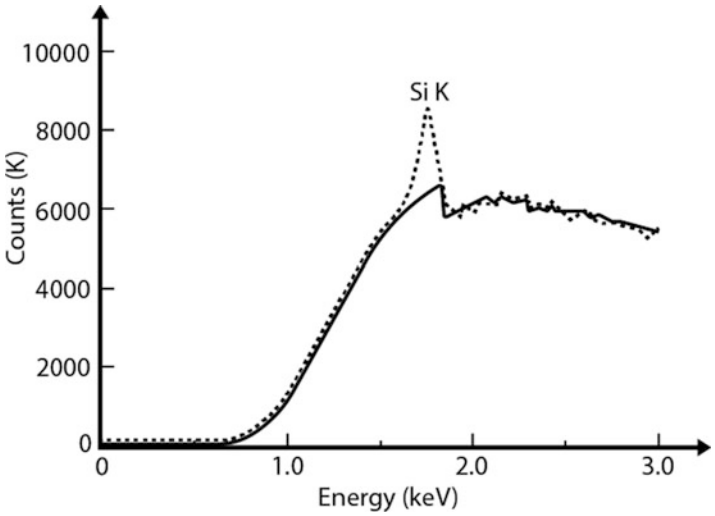

Fig. 7.12 Si internal fluorescence peak artifact in pure carbon spectrum [6]

contributes to the formation of sum peaks [6, 11]. Due to this artifact, the presence of certain elements in the test specimens was misreported in the past. With the development of more reliable electronics, these major errors are now eliminated except perhaps for very low-energy EDS analysis [6].

7.3.5 The Internal Fluorescence Peak

This artifact originates from the dead layer of the Si or Ge detector. It occurs when the x-rays entering the detector strike the detector atoms and cause them to fluoresce, resulting x-rays of Si K_{α}, Ge K, or Ge L appearing in the spectrum. This effect is known as *internal fluorescence peak* artifact. The advancements in detectors manufacturing resulted in the reduction of the thickness of dead layers which in consequence decreased the artifact of the internal fluorescence peak. Nonetheless, this artifact has not disappeared completely [6] especially when trace amounts of Si are analyzed [8, 11]. Figure 7.12 shows the internal fluorescence peak artifact.

7.4 Display of EDS Information

Information obtained from EDS analysis can be displayed in the formats summarized below.

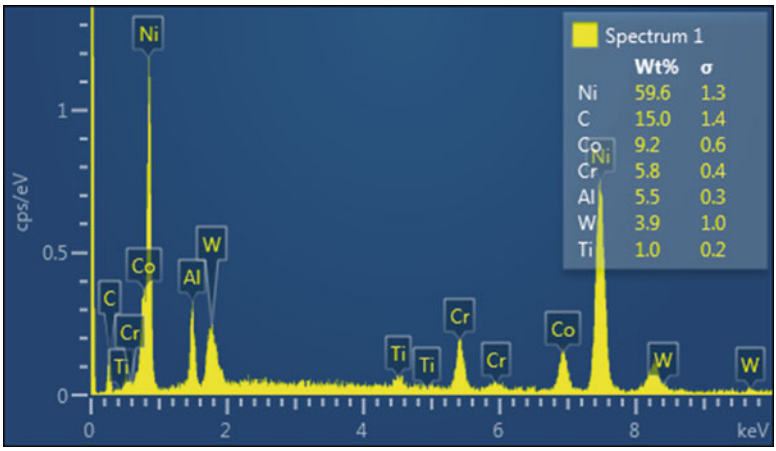

Fig. 7.13 EDS spectrum obtained from the superalloy sample showing the presence of various elements

7.4.1 EDS Spectra

The most common form of the visual format used to display microchemical information obtained from the analyzed area of a sample using EDS is the x-ray spectrum as shown in Fig. 7.13.

To obtain an EDS spectrum, the beam is usually placed over the feature of interest in the form of a focused circular spot or quadrilateral format (e.g., *spot analysis*). Irregular shapes can also be analyzed in modern microscopes. The x-rays emanating from the area of interest pass through the detector electronics, and the processed information is displayed in the form of a plot on the viewing monitor. The horizontal axis shows the energy of x-ray photons emitted from the sample, and the vertical axis shows the intensity of photons in the form of counts or counts per second. The characteristic x-rays peaks are superimposed on the background formed by continuous x-rays. The energy scale is usually displayed up to 10 keV, although it can be increased to coincide with the primary beam energy used during analysis. The EDS spectrum takes shape within a minute and serves as a quick qualitative visual indicator of the sample constitution. Further, the spectrum can be processed by the software seamlessly to display quantitative chemical information about the sample in the form of relative elemental concentrations.

7.4.2 X-Ray Maps

X-ray map displays the elemental distribution information visually in a two-dimensional plot. The process of acquiring x-ray maps is generally known as *x-ray mapping*. Area of interest is scanned by the electron beam, and from each

discrete location (pixel), an EDS spectrum is obtained and stored. The number of discrete locations and beam dwell time for acquiring EDS data from within the area of interest can be selected by the user thus controlling the final resolution of the x-ray map. The EDS data from each location is stored in the computer memory thus making it possible to recall and analyze that particular data set offline later. Multitudes of frames (sometimes up to hundred) are taken from the same area to improve map resolution. High probe currents are employed for x-ray mapping to attain good contrast.

Maps are displayed in multiple windows. Data for all elements is captured in each pixel due to which different elements can be mapped simultaneously. Each window displays the total scanned area. Each window is reserved for one element of interest only that is predetermined using spot or area EDS analysis. The area(s) that appears bright within a window is the region where a particular element (for which that window is reserved) is concentrated (see Fig. 7.14).

Alternatively, color contrast can be used in a single window for clearer visualization and better understanding (see Fig. 7.15). Primary color superposition displays images with three elements where maps are obtained by assigning color red, green, and blue, respectively. Another way is pseudocolor scales which are based on either thermal scale or on logarithmic three-band scale. In this way, elements present in a sample are colored maps of estimates of elements; each color in a window represents one element.

X-ray mapping sorts out and visualizes the elemental dispersion in a multiphase sample. X-ray mapping can be considered to be an image of the scanned area of interest formed by x-ray spectra. Images are usually produced with a file extension of TIFF. Multiple scans at extremely high magnification can produce image drift during the scan to make the topographies appear smeared in x-ray maps. The drift could distort the image even during a single scan, whereas discrepancies become noticeable when multiple scans are performed. In such a case, the operator has the option to stop and continue as appropriate rather than wait until the end of the full scan. Electron beam stability becomes important during x-ray mapping which can take anything from tens of minutes to a few hours depending on the number of elements scanned, beam dwell time, and the number of frames employed.

Continuous x-rays form part of the x-ray maps. Background in the peak constitutes roughly 6% count in major peaks. It is difficult to attain high-resolution and good detection limits during x-ray mapping, thereby precluding detection of minor or trace elements in x-ray mapping. High-resolution x-ray maps can be obtained with WDS technique but at the expense of time.

7.4.3 Line Scans

Line scanning is another type of elemental mapping where only selected area through selected line is mapped. In a line scan, probe travels linearly along a line on the specimen, and the change in count rate is measured in relation to the probe

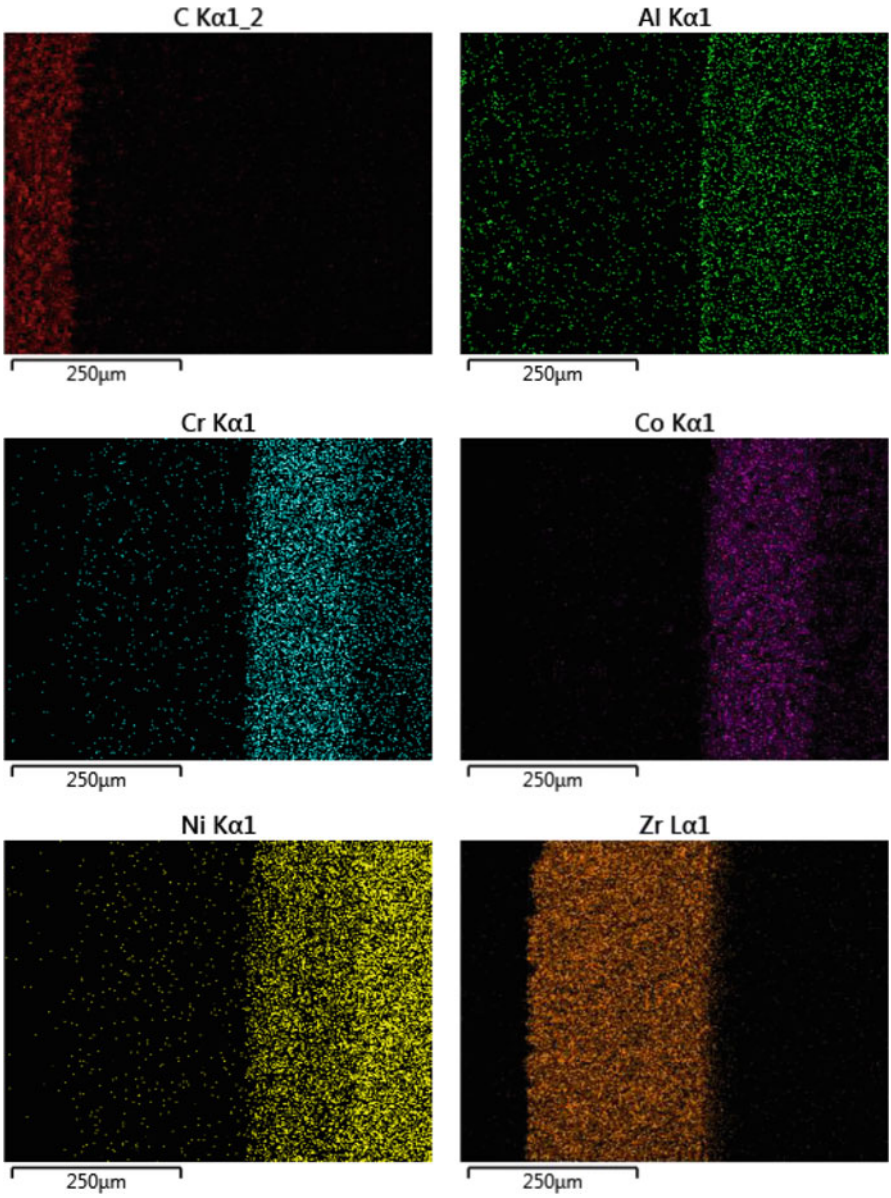

Fig. 7.14 X-ray map showing elemental distribution within the thermal barrier coating (TBC) sample. Each window represents one particular element. The bright colored region is the area of the sample where an element is concentrated

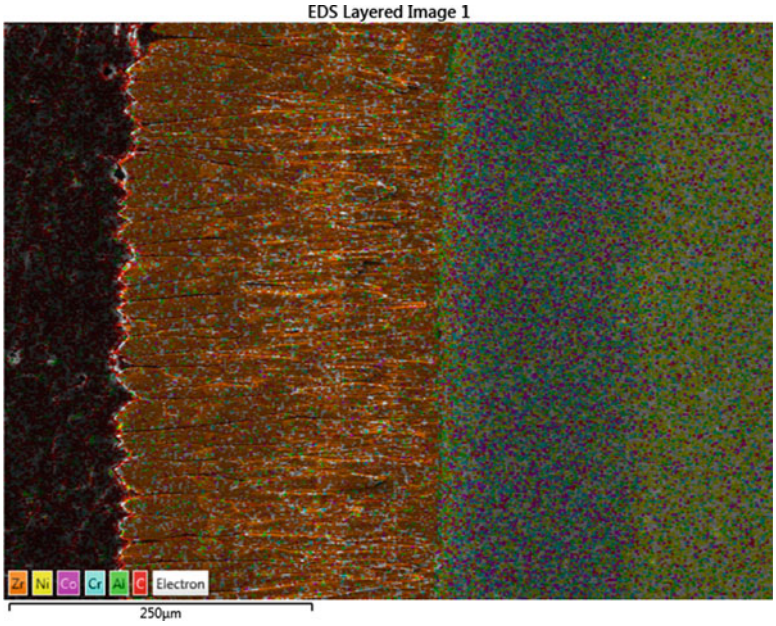

Fig. 7.15 X-ray combination map of thermal barrier coating (TBC) where window with six colors represents the extent of distribution and concentration of six different elements in one image

position. The essential variables are number of points, dwell time per location, and number of passes. Line scans are used to examine elemental variations in features such as impurities, precipitates, and grain boundaries. Similar to x-ray maps, an EDS spectrum is taken and recorded at each pixel on the selected line. An example of a line scan is given in Fig. 7.16.

7.5 Quantitative EDS Analysis

7.5.1 Introduction

Once the elements present within a specimen are identified using qualitative EDS analysis, it is generally required to determine their level of concentration. This is undertaken using quantitative EDS analysis. The concentration of an element in a specimen can be high in which case it is called a major element (generally taken as more than 10 wt%), lower concentration element is termed as minor element (1–10 wt%), and a concentration below 1 wt% is usually designated as trace element [8]. The lower limit of detection for EDS is around 0.2 wt%. The higher the concentration of an element in a specimen, the greater is the accuracy with which it can be quantified. It follows that trace elements are difficult to detect as well as hard to quantify with a high degree of accuracy. Likewise, quantification of

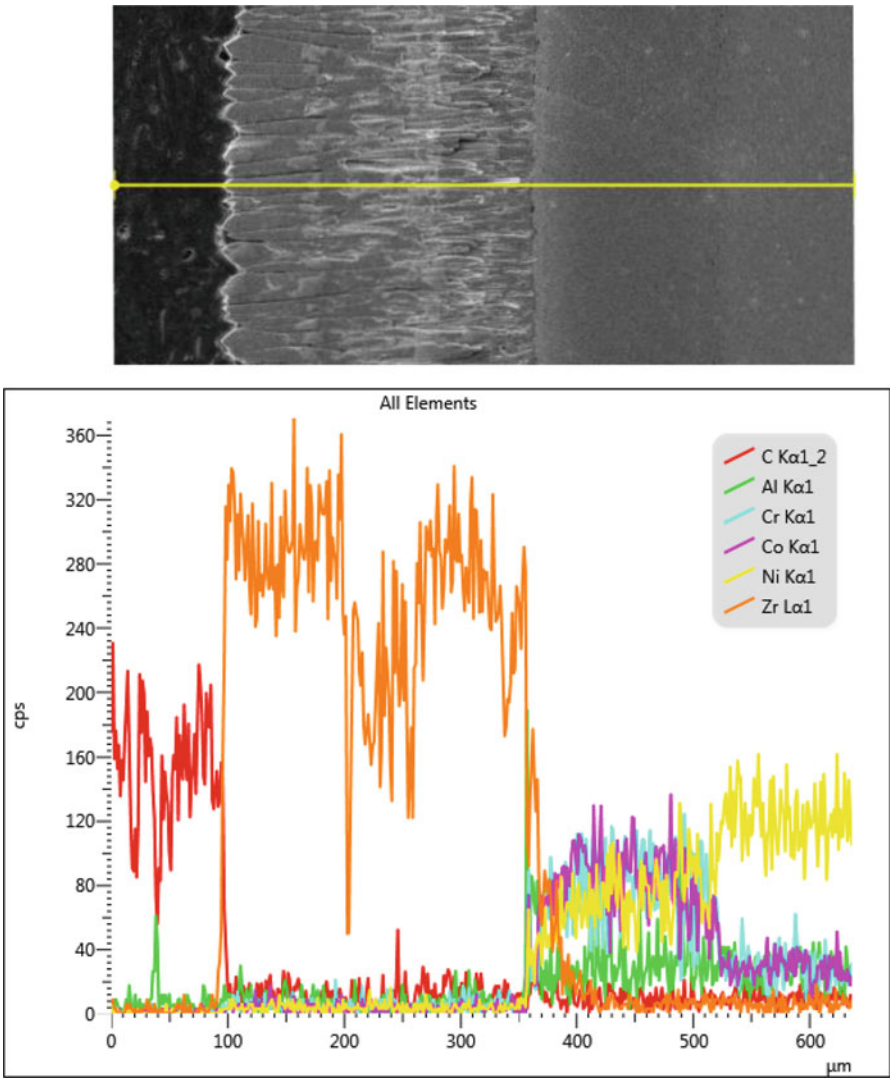

Fig. 7.16 Line scan through thermal barrier coating (TBC) sample showing variation in elemental composition of various elements along a line

concentrations of light elements presents bigger challenge compared to that of heavy elements. Generally, if correct specimen preparation and data acquisition procedures have been adopted, 1–2% accuracy of quantification is achieved using EDS analysis.

Quantitative EDS analysis can be conducted using standards or employing a standardless technique. Analysis with standards involves EDS analysis of specimens (i.e., standards) that are similar in composition to that of the unknown specimen being analyzed. Spectra obtained from the standard specimen(s) are compared with

those obtained from the unknown specimen to determine the concentration of different elements in the unknown specimen. The accuracy of such an analysis is high, but the procedure is cumbersome. Standardless EDS analysis involves testing only unknown specimen and comparing spectra with spectral data stored in the computer to quantify concentrations of elements in the unknown specimen. Such a technique is fast and convenient, but accuracy is less. Both techniques are described in the following sections. It is assumed that specimens tested are flat and polished down to 0.1 μm using standard metallographic techniques. Specimens are stable under the beam and do not undergo beam damage. They are conductive to avoid beam instability and change in x-ray intensity during analysis. It is important that optimum operating conditions are employed to obtain EDS spectra and elements in the specimen have been correctly identified using the qualitative technique as described in the previous sections.

7.5.2 EDS with Standards

7.5.2.1 Castaing's First Approximation

The standard specimen is the one which has known and uniform composition along its analyzed surface at a microscopic level. The standard specimen is selected due to its closeness in composition to that of the unknown specimen. However, this is usually not possible in practice. Therefore, mostly 100% pure elements are used as standards which work equally well for microchemical analysis. In some cases where pure elemental compositions are difficult to achieve, simple compounds such as oxides are employed as standards. Both standards and unknown specimens are prepared to the same level of finish and analyzed in the SEM using the same detector and microscope conditions such as electron beam energy, probe current, EDS detector take-off angle, analysis time, etc. If used, same thickness of the conductive coating should be applied to both standard and unknown specimen. The EDS spectra thus obtained from the standard and unknown specimens are compared. The peak intensity of an element i in the spectrum obtained from the unknown specimen relative to the peak intensity of the same element i in the standard specimen will indicate wt% concentration of element i relative to the wt% concentration of that element in the standard. If the standard is a pure element, same intensity peaks from the standard and the unknown will indicate 100 wt% concentration of element i in the unknown specimen. Similarly, half of the standard intensity will suggest 50 wt% concentration. This can be written as follows:

$$\frac{C_{i\ (\text{unknown})}}{C_{i\ (\text{standard})}} \approx \frac{I_{i\ (\text{unknown})}}{I_{i\ (\text{standard})}} = k_i \tag{7.5}$$

where

$C_{i\ (\text{unknown})}$ is weight percent concentration of element i in the unknown bulk specimen

$C_{i\ (\text{standard})}$ is weight percent concentration of element i in the standard

$I_{i\ (\text{unknown})}$ is the intensity of the characteristic x-ray peak emanating from element i in the unknown specimen

$I_{i\ (\text{standard})}$ is the intensity of the characteristic x-ray peak emanating from element i in the standard

The ratio between these the two intensities is known as "k-ratio". Equation 7.5 can be written as:

$$C_{i\ (\text{unknown})} = k_i C_{i\ (\text{standard})} \tag{7.6}$$

For pure standards, $C_{i(\text{standard})}$ equals 1. Since unknown and standard specimens are analyzed under similar conditions, k-ratio is independent of constant factors associated with the instrument and standard and unknown specimens. Weight percent concentrations of other elements in the unknown specimen are determined using k-ratio in a similar manner. k-ratio forms the basis of quantification used in EDS microchemical analysis and is obtained for each element present in the unknown specimen. Peak intensities used in the above equation are net peak intensities obtained by subtracting the peak overlaps and background from the peaks. Various methods such as linear interpolation or extrapolation, filtering, modeling, etc., can be used for background subtraction. Overlapping peaks in the x-ray spectrum need to be separated using de-convolution software programs. Adequate relative intensities should be obtained during analysis since theoretical calculations do not correct for errors in the measurement of x-ray peak intensities. Equation 7.5 above assumes that peak intensities are generated proportional to the respective concentrations of elements. This is called Castaing's first approximation to quantitative analysis.

7.5.2.2 Deviation from Castaing's First Approximation

When multielement specimens are tested, Castaing's assumption fails to hold. It is observed that the ratio of intensities do not vary linearly with the ratio of concentrations as suggested by Eq. 7.5. This is understandable since the matrix of the unknown multielement specimen is not similar to a pure standard. Due to the differences in the matrices, x-rays of a given element in the unknown specimen will undergo absorption more than the corresponding x-rays in the standard sample resulting in lowered intensities, while x-rays of another element in the unknown sample will yield stronger intensities due to a possible fluorescent effect. X-rays emanating from light elements can show strong absorption in the heavy matrix. Due to this phenomenon, measured intensities from unknown specimens need to be corrected for atomic number (Z), absorption (A), and fluorescence (F) effects to arrive at correct intensities and hence generate reliable concentration values. These effects are commonly known as *matrix effects* which can be quite large in certain material systems. The relative intensity of an element does not generally follow a linear relationship with its concentration due to matrix effects. The magnitude of the effect varies with the composition of the material analyzed.

The mostly applied correction procedure to counter matrix effects and undertake quantitative microchemical analysis is known as ZAF correction method as shown by the following equation:

$$C_{i\ (\text{unknown})} = [Z_i \times A_i \times F_i] \times C_{i\ (\text{standard})} \times \frac{I_{i\ (\text{unknown})}}{I_{i\ (\text{standard})}} = [Z_i \times A_i \times F_i]\ k_i \qquad (7.7)$$

where Z_i, A_i and F_i are correction factors for atomic number, absorption, and fluorescence effects, respectively, for element i in the specimen. Above equation is calculated separately for each element present within the specimen. The aim of matrix corrections is to convert the measured intensity from the sample relative to that from a standard to the actual concentration.

7.5.2.3 Matrix Effects

The intensity of x-rays generated from within a specimen depends on instrumental factors such as accelerating voltage and probe current used as well as specimen factors such as elastic and inelastic scattering processes occurring within a specimen. Measured or detected intensity of x-rays is not equal to generated intensity due to absorption or fluorescence of x-rays generated within the specimen. This variation between generated and detected values of x-ray intensity is governed by the composition of the specimen matrix and is known as matrix effects. Primary phenomena giving rise to matrix effects constitute effect of atomic number (Z), absorption (A) and fluorescence (F), as discussed below.

Atomic Number Effect

Backscattered electrons are those incident beam electrons that undergo elastic scattering upon entering the specimen, get deflected through large angles, and leave the specimen. Backscattered electrons represent a significant proportion of beam electrons that, as they leave the specimen surface, become unavailable to take part in ionization of specimen atoms in order to generate x-rays. Therefore, backscattered electrons do not contribute to x-ray generation within the specimen. The degree of backscattering strongly depends on the atomic number of the specimen material (see Fig. 3.14a). Specimens with high atomic number show a high degree of backscattering. In a multielement specimen, the phase with a high atomic number will eject a large number of backscatter electrons compared to a low atomic number phase. Also, since backscattered electrons constitute a significant proportion of the total energy of the incident beam, a substantial measure of that beam energy is removed from the sample upon their escape.

With regard to microchemical analysis, consider measuring the low concentration of a light element i mixed with a high concentration of a heavy element j in a multielement specimen. The large proportion of beam electrons entering the specimen shall be backscattered by heavy element j and leave the specimen. These electrons shall be unavailable to generate x-rays from within the light element i. In this way, the concentration of i shall be underestimated if its intensity is compared

with that originating from a standard with 100% pure element *i* where a high proportion of beam electrons shall be available to generate x-rays. Therefore, a correction needs to be applied to calculations for this kind of matrix effect in order to use 100% pure standards with multielement specimens to get accurate results.

The fraction of incident beam electrons which do not backscatter and remain available within the specimen to generate x-rays is termed as *R*. It follows that low atomic number specimens (such as light elements or polymeric/life sciences specimens) produce small degree of backscattered electrons and have a large value of *R*. Generation of x-rays within a specimen also depends on latter's ability to get ionized, i.e., its critical ionization potential. Specimens with low atomic numbers demonstrate low critical ionization potentials, e.g., they readily ionize compared to heavy elements and generate x-rays. In other words, light elements demonstrate a greater "stopping power" denoted as *S* (also see Sect. 3.2.3). The higher the value of *S* of a target specimen, the greater is the rate of energy loss of incident beam energy within that specimen. Thus both backscattering *R* and stopping power *S* vary inversely with atomic number *Z*. Atomic number affects the degree of backscattering and rate of electron energy loss within the specimen and thus influences the degree of x-ray generation at a given depth of specimen. This is especially important when the specimen has light element intermixed within a heavy element matrix. The correction of atomic number effect for a particular element *i* (Z_i) is obtained by dividing stopping power *S* for the sample and standard by the backscattering *R* for the specimen and standard, i.e., $Z_i = S/R$. The *S* and *R* factors go in opposite directions and tend to cancel each other out.

It can also be seen that incident beam energy has a similar effect on the values of *R* and *S*. Electrons with higher-energy backscatter more and escape specimen surface producing lower values of *R*. Similarly, stopping power of a specimen is lower for a higher beam energy giving rise to lower *S*. Therefore, *R* and *S* have an inverse proportional relationship to incident beam energy, similar to that with atomic number. Therefore the atomic number effect can be determined by calculating x-ray generation as a function of atomic number and incident beam energy. Study of Monte Carlo simulations reveal that the volume of x-ray generation decreases with increasing atomic number at constant beam energy. This is due to an increase in backscattering in high atomic number specimens which makes a large proportion of electrons unavailable for x-ray generation. In addition, critical excitation energy also increases with an increase in atomic number. The distribution of x-rays within the generated volume is also influenced by atomic number as well as by specimen depth. For convenience, the relative intensity of x-rays generated as a function of mass depth $\varphi(\rho z)$ (where ρ = specimen density, g/cm^3, and z = linear depth, cm) is measured. Mass depth takes into account density of specimens which has a strong effect on the generation of x-rays. In this method, the atomic number correction Z_i can be calculated by taking the ratio $\varphi(\rho z)$ for the standard to $\varphi(\rho z)$ of the element *i* in a specimen. Calculation of atomic number effect by this method takes into account *R* and *S* factors described above.

Absorption Effect

The depth and volume of x-ray generation increase with an increase in incident beam energy. For a given energy, x-ray generation increases with depth from the specimen surface, reaches its highest point quickly, and then falls back to low values at greater depths. This is shown schematically by $\varphi(\rho z)$ curve in Fig. 6.18. As stated previously, not all generated x-rays will reach the detector, and some proportion of it will be absorbed within the specimen matrix. Therefore, the measured intensity I will differ from generated intensity I_0 at a given depth z, and their relationship can be described by Eq. 6.12 given in Sect. 6.4.6:

$$I = I_0 \exp\left[-\left(\frac{\mu}{\rho}\right)(\rho t)\right]$$

where

I is the intensity of x-ray photons when leaving the specimen surface
I_0 is the original intensity of x-ray photons
μ is the absorption coefficient
ρ is the density of the specimen
t is the thickness of specimen traveled
ρt is the area density known also as the mass thickness

Above equation gives a measure of absorption of x-rays within a specimen matrix. It is clear that the greater the depth at which x-rays are generated, the greater is the proportion that is lost due to absorption within the specimen. Mass absorption coefficient depends on the energy of generated x-rays; therefore its value will be different for each characteristic x-ray line. It also depends on the composition of the specimen analyzed. The mass absorption coefficient of a multielement specimen is obtained by multiplying individual absorption coefficients by their mass fractions and adding them up.

Generally, correction for mass absorption is the biggest correction made during quantitative microchemical x-ray analysis. Especially, light elements such as C, N, and O are strongly absorbed in heavy matrices and need to be accounted for during calculations. X-rays might be generated at greater depths within a specimen but might not make it to the surface due to absorption. Only those x-rays that are relatively close to the surface might escape. Absorption can be decreased by using the minimum incident beam energy required to generate characteristic x-rays resulting in lesser beam penetration and lower path lengths (t) that x-rays need to traverse to reach specimen surface. Higher take-off angles also decrease x-ray path lengths and reduce the chance to get absorbed within the specimen.

Fluorescence Effect

Characteristic x-rays generated as a result of the interaction between the electron beam and the specimen can be absorbed within the specimen matrix and cause ionization of atoms resulting in the emission of further characteristic x-rays. This fluorescent effect takes place only if the critical excitation energy of absorbing atoms

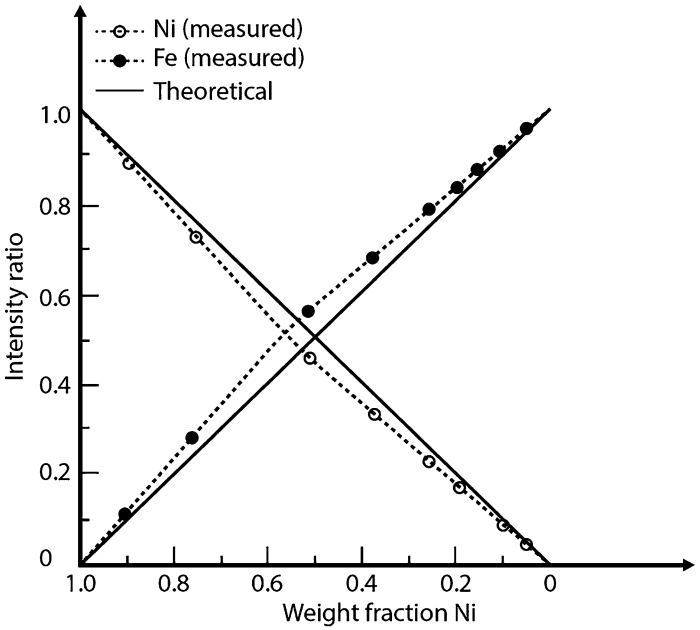

Fig. 7.17 Plot showing measured *k*-ratios (curved lines) versus weight fractions (straight lines) of Ni-Fe alloy. Adapted from [8]

is less than the energy of generated x-rays. This effect will result in an increase in the measured x-ray intensity by the SEM detector since now both the original x-rays and the x-rays generated due to fluorescence are measured. Intensity will be increased by both continuum and characteristic x-ray; however, the effect of former can be considered negligible. Correction required due to florescence effect is usually smaller compared to that for atomic number and absorption in ZAF corrections. In some cases, fluorescence can result in erroneous peaks in the x-ray spectrum.

As an example, the effect of matrix on the intensity of Fe K_α and Ni K_α characteristic x-rays in Fe-Ni alloy is shown in Fig. 7.17. If Castaing's first approximation holds, the plot should be linear. However, the measured intensity of Fe K_α is higher than theoretical value due to fluorescence induced by Ni K_α, i.e., Fe will be overrepresented. On the other hand, the intensity of Ni K_α is lower than that calculation based on Castaing's first approximation as it is absorbed by the matrix more than in the standard, i.e., Ni will be underrepresented. Such an effect needs to be compensated during calculations. Greatest deviation from a linear relationship is seen in cases where analysis is performed for light elements in a heavy matrix or light elements in a light matrix.

7.5.2.4 ZAF Iterative Process

The aim of quantitative analysis is to determine the composition of an unknown sample. The extent of matrix effects, and its required correction depends on the composition of the unknown sample. Since the composition of the sample is not

known in the first instance, the ZAF correction factors are also unknown. Therefore, true concentrations are achieved by an iterative process. In this procedure, *k*-ratio is calculated from measured intensities and used as an initial estimate of the composition of the unknown sample. Based on this *k*-ratio, ZAF factors for this composition are calculated. The composition of the unknown sample is calculated by multiplication of *k*-ratio and corresponding ZAF factors calculated in the previous step. Based on this newly calculated composition, a new set of ZAF factors are calculated. The composition of the unknown sample is again calculated by multiplying the new set of ZAF factors with the original *k*-ratio. This process continues until concentration does not change appreciably from the previous one as shown below:

First iteration: $k\text{-ratio} \rightarrow (\text{ZAF})_1 \rightarrow C_1 = k \times (\text{ZAF})_1$
Second iteration: $k\text{-ratio} \rightarrow (\text{ZAF})_2 \rightarrow C_2 = k \times (\text{ZAF})_2$
Third iteration: $k\text{-ratio} \rightarrow (\text{ZAF})_3 \rightarrow C_3 = k \times (\text{ZAF})_3$
*n*th iteration: $k\text{-ratio} \rightarrow (\text{ZAF})_n \rightarrow C_n = k \times (\text{ZAF})_n$
The procedure stops when $C_n = C_{n\text{-}1}$

7.5.2.5 Phi-Rho-Z Correction Method

Production of x-rays varies with the depth of the specimen. Phi-Rho-Z function $\phi(\rho z)$ was developed to take into account the generation of x-rays as a function of depth and self-absorption. This function uses mass depth ρz parameter instead of simple linear z (see Sects. 6.4.4 and 6.4.5). The $\phi(\rho z)$ function is defined as the x-ray intensity generated in a thin layer at some depth z, relative to the intensity generated in an isolated layer of the same thickness. This is then integrated over the total depth where the incident electrons exceed the binding energy of that particular characteristic x-ray. The curve of $\phi(\rho z)$ versus ρz is generated for each characteristic x-ray (see example in Fig. 6.18). The shape of the curve depends on accelerating voltage, the critical excitation energy of a particular element x-ray line, and mean atomic number of the specimen [9]. These curves are generated using the *tracer method*. $\phi(\rho z)$ is an elemental quantification method based on the matrix and includes fluorescence correction. The common $\phi(\rho z)$ method depends on standardization or reference measurements. Compared to ZAF, the $\phi(\rho z)$ methods have improved the accuracy of microanalysis. They involve complex computations but perform much better with light element analysis.

7.5.3 Examples of ZAF Correction Method

Quantification of the effects of atomic number, absorption, and fluorescence on the concentrations of various elements present within a multielement specimen has been undertaken and refined by various researchers in the past few decades [12–17]. X-ray intensity ratios of the unknown specimen to that of the standard specimen are measured and corrected for *Z*, *A*, and *F* effects for each element to get final values of concentrations, as shown by the Eq. 7.7 ($C_{i\ (\text{unknown})} = [Z_i \times A_i \times F_i]\ k_i$). This section includes an example of ZAF corrections taken from the literature [18].

7.5.3.1 Stainless Steel

The following example is reproduced from reference [18].

Actual composition (wt%): 62.03Fe, 23.72Cr, 13.26Ni, 0.23Mn, and 0.37Si
Standards: Pure Fe, Cr, Ni, Mn, and Si
Accelerating voltage: 25 kV
Detector take-off angle: 30°

Results of ZAF corrections for each element are shown in Table 7.1.

It can be seen from Table 7.1 that if concentrations are calculated based on mere *k* intensity ratios, the relative error in calculated concentrations would be high. The accuracy of measurements increases when ZAF corrections are incorporated into the measurements. For instance, x-ray intensity of Fe K_α line emanating from the specimen is lower than that suggested by *k*-ratio due to atomic number and absorption, while it is higher than *k*-ratio due to fluorescence of Fe K_α by Ni K_α x-rays. The overall effect is lowered intensity which is then corrected by multiplying by $[ZAF]_{Fe}$ factor of higher than 1 (e.g., 1.0235). This compensates for low measured intensity and results in concentration values closer to the actual composition than that suggested by *k*-ratios. Corrections for other elements are performed in a similar manner. The intensity of Cr k_α is enhanced due to fluorescence by K_α x-rays from Fe and Ni elements present in the specimen which results in an increased overall intensity for Cr. This is corrected by multiplying with $[ZAF]_{Cr}$ factor of less than 1 (e.g., 0.9125). For Ni, there is no fluorescence effect due to other elements present in the specimen thus requiring no correction. For this reason, F_{Ni} factor for Ni K_α is taken as 1. Silicon is heavily absorbed in the specimen and is compensated by a relatively large absorption (A_{Si}) correction. It is also clear from the table that calculations of elements present in the specimen with low concentrations (such as Mn and Si) will yield higher relative errors indicative of the challenges to quantifying such level of concentrations with a high degree of accuracy. For quantitative analysis using standards, the user needs to measure the net intensity of x-ray peaks from the standard and unknown specimen to derive *k*-ratios. ZAF correction factors are stored in computer memory, and once *k*-ratio values are entered into the computer, it can calculate elemental concentrations. ZAF factors are obtained from methods developed by various researchers over the years.

7.6 Standardless EDS Analysis

Quantitative EDS analysis with standards is carried out by analyzing unknown specimens and known standard specimens under similar measurement conditions to cancel out any differences arising due to detector efficiency. However, analysis with standards is cumbersome since intensities of all x-ray peaks need to be obtained from both known and unknown specimens in order to calculate intensity (*k*) ratios. To circumvent this requirement and for the sake of convenience, the microchemical analysis is usually undertaken using *standardless* EDS analysis. In this method,

Table 7.1 Use of ZAF correction method to analyze concentrations of the stainless steel specimen

Element (K_α lines)	k intensity ratios	Z_i factor	A_i factor	F_i factor	$Z_iA_iF_i$	Measured composition, wt% $C_i = [Z_iA_iF_i]\,k_i$	Relative error, % [a]$(C_{act.} - C_{mea.})/C_{act.} \times 100$
Fe	0.6076	1.0030	1.0316	0.9892	1.0235	0.6219 (62.19 wt%)	0.26
Cr	0.2586	0.9970	1.0070	0.9089	0.9125	0.2360 (23.60 wt%)	0.51
Ni	0.1238	0.9940	1.0804	1	1.0739	0.1330 (13.3 wt%)	0.30
Mn	0.0024	1.018	1.0014	0.9926	1.0118	0.0024 (0.24 wt%)	4.35
Si	0.0024	0.8360	1.8144	1	1.5168	0.0036 (0.36 wt%)	2.70

[a]$C_{act.}$ = Actual composition, $C_{mea.}$ = Measured composition

physical standards (specimens with known composition) are not examined by the user, and only unknown specimen is analyzed. Since the need to analyze standards is eliminated, the whole process of analysis becomes simple and efficient. X-ray peak intensities from standards are still required to estimate elemental concentrations, but these are obtained from theoretical calculations. This procedure is called *first principles standards analysis*. Alternatively, intensities are acquired from standard x-ray spectra stored in the computer. This method is known as *fitted standards standardless analysis*.

7.6.1 First Principles Standardless Analysis

The accuracy with which the intensity can be calculated depends on several critical physical parameters such as the ionization cross section, the x-ray self-absorption inside the target, the fluorescence yield, the backscatter loss, the stopping power, and the detector efficiency. Values of K shell ionization cross sections published in the literature show a variation of more than 25%, especially in the low overvoltage range, $1 \leq U \leq 3$, which is the primary operating range of energy dispersive x-ray spectrometry. Similarly, published K shell fluorescence yield shows a variation of 25% for many elements. Similar data variation is observed for L and M shell transitions. The EDS detector efficiency can also present a major source of error in the standardless analysis because characteristic x-rays of different energies are compared. Due to these reasons, use of standard intensities derived from theoretical calculations generally results in a large relative error in measured elemental concentrations. Due to this reason, this method is seldom employed, and the most commonly used procedure is to derive standard intensities from stored x-ray spectra.

7.6.2 Fitted Standards Standardless Analysis

In this method, the intensity values are obtained from experiments performed on a range of standards consisting of pure elements or binary compounds. A library of intensities for K, L, and M x-ray peaks is obtained for elements ranging from low to high atomic numbers. This results in a database of standard x-ray spectra intensities. Change in x-ray intensities with atomic number is modeled, and mathematical fits are derived to predict the intensity of an element with a specific atomic number. Similarly, the change in x-ray intensities with accelerating voltage can be modeled and dependence of elemental concentration on beam energies is calculated. This modeling is performed at the manufacturers' site and is not undertaken by the SEM user. Intensities of standard spectra obtained at the factory and stored in the computer are adjusted according to the efficiency of individual EDS detector fitted on a particular SEM. The term *standardless* in this procedure to obtain elemental concentrations can be regarded as a misnomer since x-ray intensities used in calculations are actually derived experimentally from physical standards. Perhaps, it came to be known as standardless technique since SEM operators do not measure

intensities from standard specimens and only analyze unknown specimens. The accuracy obtained from this procedure can be several orders of magnitude higher than that obtained from standard intensities using theoretical calculations. Accuracy is greater in specimens with similar atomic numbers and for those where only K_α peak is measured. Accuracy decreases with use of L or M peaks for intensity measurements. All results are normalized to 100%, and oxygen is calculated by the direct method or indirectly by the stoichiometric method.

7.7 Low-Voltage EDS

The high voltage and large beam-specimen interacting volume of traditional EDS set-up leads to low spatial resolution of the detecting elements, low detectability of lighter elements (lighter than Be), and the high interaction between beam and specimen may cause beam damage to the sample. More recently, low-voltage EDS (LV-EDS) technique was developed as a microanalysis tool which overcomes the above-stated drawbacks. In this technique, an electron beam energy of <5 keV is used to undertake microanalysis with high spatial resolution, which can be termed as "nano-analysis." LV-EDS can be used for compositional analysis where WDS cannot be applied due to latter's use of high current (tens of nA) during analysis even though the energy resolution of WDS is much better than EDS. The higher current is said to lead to thermal damage and degradation of spatial resolution [19]. In addition, LV-EDS reduces x-ray absorption, thus increasing the accuracy of the quantitative analysis.

More recently, microcalorimeters equipped with enhanced detectors and open windows to extend the sensitivity of the low-voltage characteristic spectrum have been developed. Some of these microcalorimeters are mounted on the SEM itself. In FE-SEM, with the application of LVEDS, elemental mapping of bulk materials at high spatial resolutions has been possible [20]. Commercial μcal EDS detectors have higher peak-to-background ratios, fewer peak overlaps and where peaks do overlap, the detection is improved more than that of conventional EDS detectors [20].

When accelerating voltage used is less than 5 kV, the L and M lines of heavy elements are closely spaced with the K lines of lighter elements. These peaks are then not easily distinguished using the SSD (solid-state detectors) which has a resolution of about 122 eV. To overcome this limitation, an EDS system was developed based on a transition edge x-ray sensor (TES) which has a much higher-energy resolution of less than 20 eV [19]. The best energy resolutions demonstrated by low-voltage EDS technology is said to be 2.0 eV FWHM at 1.5 keV (Al-Kα) and 2.4 eV FWHM at 5.9 keV, i.e., the Mn-Kα using a μcal EDS system [21].

One obvious disadvantage is that elements with high critical ionization potential cannot be detected at low voltages. Peak overlap is another drawback. Moreover, contamination buildup at the specimen surface can seriously hamper accurate quantitative analysis at low kV.

Examples of applications of LV-EDS include composition analysis of interplanetary dust particles [20], oxide surface analysis [20], oxidation-state measurements [21], depth profiling of multilayered films [22], and nano-analysis of semiconductor device [23].

7.8 Minimum Detectability Limit (MDL)

The minimum concentration of an element that can be detected in a specimen is called its *minimum detectability limit* (MDL) or *sensitivity*. For an element to be detected, its characteristic peak needs to visible over its background. Normally, it is assumed that peak is detectable if it is at least two times the mean variation height (standard deviation) of the background, i.e., $2\sqrt{I_b}$ where I_b is the intensity of the background, i.e., mean count level of background and $\sqrt{I_b}$ is the variation or noise about this mean. The minimum detectability limit of an element can be expressed as follows:

$$\mathrm{MDL} \propto \frac{1}{\sqrt{I_p \left(\frac{I_p}{I_b}\right) t}} \tag{7.8}$$

where

I_p is the peak intensity of the x-ray line
I_b is the background intensity
t is the acquisition time

It is clear that better sensitivity can be increased by increasing peak-to-background ratio and acquisition time.

7.9 Wavelength Dispersive X-Ray Spectroscopy (WDS)

The characteristics x-rays produced due to specimen-beam interaction have wavelengths unique to the elements in the specimen. This forms the basis for the qualitative as well as quantitative analysis using wavelength dispersive x-ray spectroscopy (WDS). The wavelength of the x-ray photons provides an avenue for the identification of elements in the sample, and the x-ray peak provides the basis for quantification after taking into account numerous factors that determine peak area.

7.9.1 Instrumentation

The primary instrument used to carry out wavelength dispersive x-ray spectroscopy (WDS) is known as electron probe microanalyzer (EPMA) which is very similar to SEM. EPMA employs electron source (W filament, LaB_6 emitter, or field emission

Fig. 7.18 Photograph of electron probe microanalyzer (EPMA) fitted with two wavelength dispersive (WD) x-ray spectrometers

gun), electron column equipped with electromagnetic lenses and apertures, specimen chamber with E-T/BSE detectors and allied vacuum equipment very similar to that in the SEM. The electron beam is generated and accelerated through the column. It is scanned onto the surface of the specimen in the form of a raster. The interaction between specimen and electron beam produces secondary and backscattered electrons as well as characteristic and continuous x-rays. The electrons are used to form SE and BSE images, while the x-rays are used for microchemical analysis. The only difference is that EPMA employs high probe current (typically tens of nanoamperes) and wavelength dispersive x-ray spectrometers instead of energy-dispersive x-ray spectrometer to undertake the chemical analysis. These WD spectrometers are fitted in the ports available in the EPMA specimen chamber. The number of these spectrometers could range from 2 to 4. A photograph of EPMA with 2 spectrometers is shown in Fig. 7.18.

7.9.2 Working Principle

The working principle of EPMA is illustrated in a simplified schematic shown in Fig. 7.19. The electron beam is generated at the top of the electron column. It is accelerated toward the specimen. Typical accelerating voltage used is 20–30 kV. Upon striking the specimen surface, x-ray signals are produced which are directed toward a curved crystal with known interplanar spacing (*d*-spacing). The x-rays are reflected off the crystal and directed into a detector. The difference here compared to the SEM-EDS technique is that the x-rays do not enter the detector directly upon

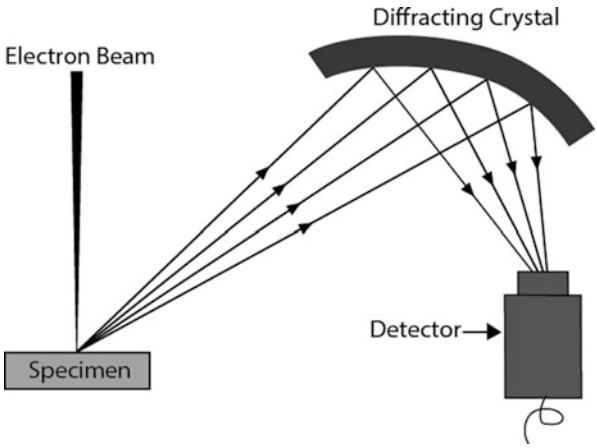

Fig. 7.19 Schematic illustrating basic instrumental setup used in wavelength dispersive spectroscopy (WDS) in the electron probe microanalyzer (EPMA)

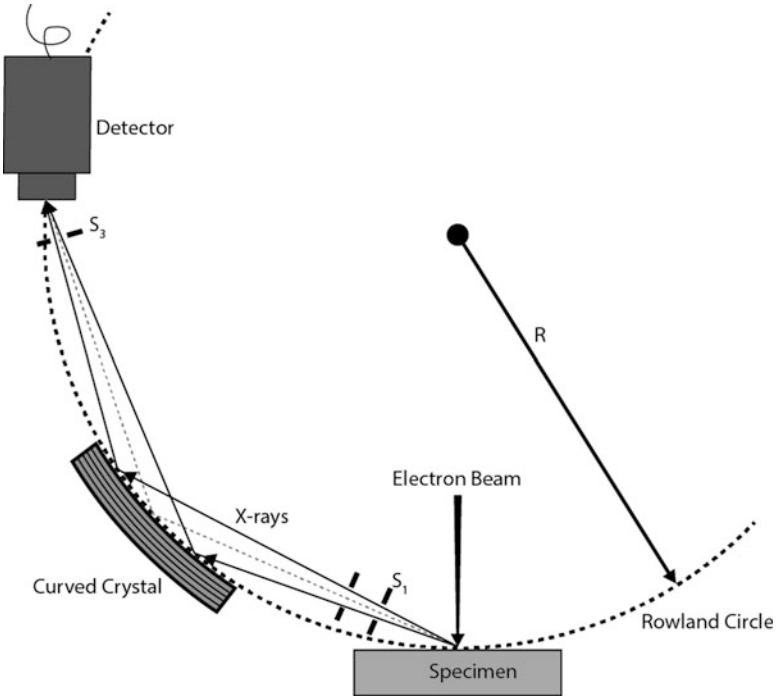

Fig. 7.20 Schematic showing the working principle of the WDS technique [24]

ejection from the sample. X-rays are reflected off the surface of a crystal before being directed into the detector.

The sample, crystal, and the detector are positioned on a circle (called Rowland circle) as shown in Fig. 7.20. The sample is located at the bottom of the specimen chamber. The crystal and the detector are made to move on the Rowland circle

during analysis. During this movement, the distance between the crystal and the specimen is always kept equal to the distance between the crystal and the detector. The movement of the crystal on the circle serves to continuously change (from low to high) the angle θ at which the x-rays are incident on the crystal. The characteristic x-rays with specific wavelength emanate from the constituent elements of the sample due to orbital transitions and strike the surface of the crystal that has a fixed d-spacing. During the course of crystal movement, it is probable that x-rays (with specific λ) emanating from a particular element in the specimen and upon the striking the crystal (with fixed d) at an angle θ satisfy Bragg's equation (see Eq. 5.3, $n\lambda = 2\ d \sin\theta$) resulting in diffraction.

Upon diffraction, the amplitude of the x-rays will increase manifold resulting in an increase in the intensity of the x-rays at the diffraction angle θ. This increase in intensity is measured by the detector and appears as a peak in the x-ray spectrum recorded in the computer. The movement of the crystal is precisely controlled and monitored thereby providing an exact measure of θ at the time of diffraction. The d value is identified as the crystal used is known. From Bragg's equation, λ is then measured. Working backward, the element that emanates the x-ray with this particular wavelength is identified as the λ is specific to that element. The crystal is moved from low to high θ values, and any diffracted x-rays are detected during this run. In this way, qualitative identification of the elements is carried out. One type of crystal is unable to detect a vast array of possible wavelengths from small to large that encompass the majority of elements in the periodic table. Therefore, two crystals (installed back to back) are used in each spectrometer. Only one crystal can reflect x-rays at a given time. After the first run is completed through all θ angles, the crystals are flipped, and the second crystal with a different d-spacing starts to receive the signals from the specimen. The number of spectrometers coupled to the EPMA can be as high as four. Two crystals installed in two different spectrometers can receive x-ray signals simultaneously. In case of four spectrometers, four crystals (all with different d-spacing) can process the signal at the same time concurrently producing four x-ray spectra on the viewing monitor.

X-ray signal in electron beam instruments is weak. The signal is maximized by using fully focusing x-ray spectrometers with curved analyzing crystals. The two basic types of crystal geometries used in the WDS setup are called *Johann* geometry and *Johansson* geometry. In Johann geometry, the bending curvature of the diffracting crystal is twice the radius of the focusing circle ($2R$), also termed as the Rowland circle as shown in Fig. 7.20. In Johansson geometry, the crystal is bent to have a curvature of radius equivalent to a distance $2R$. It is also surface finished to a distance equivalent to R. This ensures that all x-rays are reflected onto the Rowland circle. In this way, x-rays are deflected off a wider crystal area and are still focused on a single point in the x-ray detector. An optical microscope is mounted to adjust z-position of the sample so that the sample is kept in full focusing condition.

The spectra generated using WDS are normally displayed in the units of sin θ, wavelength, or millimeters of the crystal movement. This is in contrast to a rather more convenient one of EDS that gives the spectra in intensity as a function of energy. Because of this, some systems allow for the transformation of WDS spectra

from the stated units to energy units. WDS is characterized by high-energy resolution typically 10 eV in contrast to 122 eV in EDS.

7.9.3 Analytical Crystals

The range of Bragg angles used in WDS instrument is limited by available space. The maximum achievable θ angle in a WDS system is in the range of 67–73°. Thus, the maximum λ of characteristic x-rays being diffracted is less than $2d$ of the analyzing crystal. Thus, crystals with a wide range of d-spacing values are necessary to cover the entire range of x-ray wavelengths of interest (~0.1 to 2.0 nm). Usually, microprobes employ multiple crystals in each spectrometer to increase analytical flexibility; each spectrometer has a pair of crystals that can be flipped. The most commonly used crystals include lithium fluoride (LiF), thallium acid phthalate (TAP), pentaerythritol (PE), and layered synthetic microstructure (LSM). LIF is an ionic solid, while PET and TAP are organic crystals. X-rays having a long wavelength (low energy) require larger crystal-lattice spacing to obtain optimum diffraction, and hence the layered synthetic microstructure crystal remains a better option. The pseudocrystals are usually produced by depositing vapor on the alternating crystal-lattice layers of the lighter and that of the heavier elements. The selection of the elements is made in order to achieve maximum scattering efficiency; also the width of the alternating layers provides real d-spacing [25].

A given x-ray line can be diffracted by more than one crystal, but the limited space within the spectrometer dictates the most suitable crystal that can be used for this purpose. For example, Fe-K_α with a wavelength of 0.1937 nm is located at θ of 28.75° on LIF, 12.8° on PET, and 4.3° on TAP. Fe-K_α radiation falls at values of θ which are either very near or beyond the mechanical limits of spectrometer's movement for PET and TAP, thus necessitating the use of LIF crystal. Other important characteristics of an analyzing crystal apart from interplanar (d) spacing include stability, reflectivity, spectral range, spectral resolution, and thermal expansion coefficient [26].

7.9.4 Detection of X-Rays

Gas proportional counters are the most common detectors used in WDS for low-energy lines. In this type of detectors, the sample-generated x-rays enter the detector via a collimator and get absorbed by atoms of counter gas in the detector. The atoms of the counter gas, in turn, emit photoelectron on absorbing the x-rays. Finally, the produced photoelectrons are accelerated to a wire located at the center of the tube for further ionization that will generate an electrical pulse having an amplitude proportional to the energy of the x-ray photons generated by the specimen. Theoretically, 16 eV is required to generate one electron pair, but up to about 28 eV is ordinarily required for effective electron pair production. Therefore, the

number of electron pair produced should be a value obtained after dividing the energy (eV) by this number.

Another type of detector which is mostly used in high-energy x-ray lines is the sealed proportional counter detector. This type of detector has a thicker window (slit; Mylar) compared to its gas flow counterpart. The ionization gas widely used in sealed proportional counters is Xenon (Xe) gas or Xe-CO_2.

7.9.5 Advantages/Drawbacks of WDS Technique

7.9.5.1 Advantages

Nondestructive technique
High-energy resolution (~5–10 eV)
High peak-to-background ratios (10,000:1)
Good detection efficiency for all x-rays
Fast counting rates
Good detection of light element
Better trace element detection compared to EDS
Suitable for different synthetic and natural solid minerals
The capability of x-ray mapping of elements using *rastered* electron beam

The WDS systems can resolve relative changes in wavelength ($\Delta\lambda/\lambda$) in the range 0.002–0.02 corresponding to the energy range 0.01–0.1 keV. This energy resolution value is >10× better than that of EDS. Modern WDS systems can detect elements from upward of C ($Z = 6$).

7.9.5.2 Disadvantages

Complex mechanical/moving components
Complicated analysis
Operator intensive/time-consuming analysis
Specimen height-dependent focus
Limited solid angles (<0.01 limited solid angles)
Serial detection
Expensive
Low atomic number elements (H, He, Li, and Be) cannot be analyzed using WDS, and hence numerous geologically important materials cannot be measured
Even though WDS has enhanced elemental peaks spectral resolution, some significant peak overlaps still exists (e.g., Vanadium-K_α and Titanium-K_β)
WDS technique does not distinguish different isotopes of elements
The quantification process requires the use of standard reference materials, which makes the method relatively expensive

7.9.6 Qualitative WDS Analysis

In WDS, elements identification in specimens is achieved by obtaining the angles that satisfy the Bragg's law as the scan runs through a range of angles during analysis. The peaks of elements appear at the angles θ where Bragg's law is satisfied. The spectra generated using WDS are given in intensity (y-axis) versus sin θ, x-ray wavelength, or millimeters of the crystal movement (x-axis). This is in contrast to EDS that gives the spectra in intensity versus x-ray energy. Procedure to undertake qualitative WDS is summarized below:

- Peak acquisition begins at the shortest wavelength end of the crystal spectrum corresponding to the highest photon energy. This enhances the chances of obtaining a first-order peak ($n = 1$).
- The wavelength of the resulting peak is determined by selecting peak with the highest intensity.
- As soon as the element in the specimen is identified, all possible high-order peaks related with each first-order peak throughout the set of crystals are identified.
- After this, the next unidentified high-intensity, the low-wavelength peak is examined. This procedure is repeated for each peak.

References

1. Fitzgerald R, Keil K, Heinrich KFJ (1968) Solid-state energy-dispersion spectrometer for electron-microprobe x-ray analysis. Science 159:528–530
2. Torma P, Sipila H (2013) Ultra-thin silicon nitride X-ray windows. IEEE Trans Nucl Sci 60:1311–1314
3. Torma PT, Kostamo J, Sipila H, Mattila M, Kostamo P, Kostamo E, Lipsanen H, Laubis C, Scholze F, Nelms N, Shortt B, Bavdaz M (2014) Performance and Properties of Ultra-Thin Silicon Nitride X-ray Windows. IEEE Trans Nucl Sci 61:695–699
4. Lee C, Wei X, Kysar JW, Hone J (2008) Measurement of the elastic properties and intrinsic strength of monolayer graphene. Science 321(5887):385–388
5. Huebner S, Miyakawa N, Kapser S, Pahlke A, Kreupl F (2015) High performance X-ray transmission windows based on graphenic carbon. IEEE Trans Nucl Sci 62(2):588–593
6. Williams DB, Carter CB (2009) Transmission electron microscopy: a textbook for materials science, 2nd edn. Springer, New York, USA
7. Williams DB, Goldstein JI, Newbury DE (1995) X-Ray spectrometry in electron beam instruments, 1st edn. Springer, New York, USA
8. Goldstein JI, Newbury DE, Joy DC, Lyman CE, Echlin P, Lifshin E, Swayer L, Michael J (2007) Scanning electron microscopy and X-Ray microanalysis, 3rd edition (Corrected edition), Springer, New York, USA
9. Reed SJB (1993) Electron microprobe analysis and scanning electron microscopy in geology, 2nd edn. Cambridge University Press, Cambrdige, UK
10. Zhou W, Wang ZL (2006) Scanning microscopy for nanotechnology. Springer, New York, USA
11. Hawkes PW, Spence JCH (2008) Science of microscopy, vol 1. (corrected printing. Springer, New York. USA

12. Castaing R (1951) Application of electron probes to local chemical and crystallographic analysis, Ph.D. Thesis, University of Paris, Paris. France. English (trans: Duwez P and Wittry DB) California Institute of technology, 1955
13. Duncumb P, Reed SJB (1968) Progress in the calculation of stopping power and backscatter effects. In: Heinrich KFJ (ed) Quantitative electron probe microanalysis. National Bureau of Standards Special Publication 298, US Government printing office, Washington D.C., p 133
14. Bastin GF, Heijligers HJM, Van Loo FJJ (1986) A further improve- ment in the Gaussian $(pz) approach for matrix correction in quantitative electron probe microanalysis. Scanning 8:45–67
15. Philibert J (1963) In: Pattee HH, Cosslett VE, Engstrom A (eds) Proceedings of the 34th international symposium on X-ray optics and X-ray microanalysis. Academic Press, New York, p 379
16. Duncumb P, Shields PK (1966) Effect of critical excitation potential on the absorption correction. In: McKinley TD, Henrich KFJ, Wittry DB (eds) The electron microprobe. John Wiley & Sons, New York, p 284
17. Reed SJB (1965) Characteristic fluorescence corrections in electron-probe microanalysis. Br J Appl Phys 16(7):913
18. Toya T, Kato A, Jotaki R (1984) Quantitative analysis with electron probe microanalyzer. JEOL Training Center, JEOL Ltd., Tokyo, p 83
19. Tanaka K (2006) A microcalorimeter EDS system suitable for low acceleration voltage analysis. Surf Interface Anal 38:1646–1649. https://doi.org/10.1002/sia.2408
20. Kenik EA, Demers H (2006) Spectrum imaging with a microcalorimeter EDS detector on a FEG-SEM Cr Mn 1 μm. Met Mater 12(Supp 2):140–141. https://doi.org/10.1017/S143192760606658X
21. Cantor R, Croce MP, Havrilla GJ, Carpenter M, McIntosh K, Hall A, Ullom JN (2016) Oxidation state determination from chemical shift measurements using a cryogen-free microcalorimeter X-ray spectrometer on an SEM. Microsc Microanal 22(S3):434–435. https://doi.org/10.1017/S1431927616003020
22. Rickerby DG (1999) Application of low voltage scanning electron microscopy and energy dispersive X-Ray spectroscopy. In: Chapter from book impact of electron and scanning probe microscopy on materials research. Springer, New York, pp 367–385
23. Redfern D, Nicolosi J, Weiland R (2002) The microcalorimeter for industrial applications. J Res Natl Inst Stand Technol 107(6):621–626
24. Goodhew PJ, Humphreys J, Beanland R (2001) Electron microscopy and analysis. Taylor and Francis, London
25. Marco S, Ivan B (2006) An introduction to energy-dispersive and wavelength-dispersive X-ray microanalysis. Microsc Anal 20(2):S5–S8 (UK)
26. René EVG, Andrzej AM (2002) Handbook of X-ray spectrometry, 2nd edn, Revised and expanded. Marcel Dekker, Inc., New York, ISBN: 0-8247-0600-5